

# Formation of miarolitic-class, segregation-type pegmatites in the Taishanmiao batholith, China: The role of pressure fluctuations and volatile exsolution during pegmatite formation in a closed, isochoric system

YABIN YUAN<sup>1,2,4</sup>, LOWELL R. MOORE<sup>2</sup>, RYAN J. MCALEER<sup>3,†</sup>, SHUNDA YUAN<sup>1</sup>, HEGEN OUYANG<sup>1</sup>, HARVEY E. BELKIN<sup>3</sup>, JINGWEN MAO<sup>1</sup>, D. MATTHEW SUBLETT JR.<sup>2</sup>, AND ROBERT J. BODNAR<sup>2,\*;‡</sup>

<sup>1</sup>MLR Key Laboratory of Metallogeny and Mineral Assessment, Institute of Mineral Resources, Chinese Academy of Geological Sciences, Beijing 100037, China

<sup>2</sup>Department of Geosciences, Virginia Tech, Blacksburg, Virginia 24061, U.S.A.

<sup>3</sup>U.S. Geological Survey, 12201 Sunrise Valley Drive, Reston, Virginia 20192, U.S.A.

<sup>4</sup>Department of Earth and Space Sciences, Southern University of Science and Technology, Shenzhen, Guangdong 518055, China

## ABSTRACT

The Taishanmiao granitic batholith, located in the Eastern Qinling Orogen in Henan Province, China, contains numerous small (mostly tens of centimeters in maximum dimension) bodies exhibiting textures and mineralogy characteristics of simple quartz and alkali feldspar pegmatites. Analysis of melt inclusions (MI) and fluid inclusions (FI) in pegmatitic quartz, combined with Rhyolite-MELTS modeling of the crystallization of the granite, have been applied to develop a conceptual model of the physical and geochemical processes associated with the formation of the pegmatites. These results allow us to consider the formation of the Taishanmiao pegmatites within the context of various models that have been proposed for pegmatite formation.

Field observations and geochemical data indicate that the pegmatites represent the latest stage in the crystallization of the Taishanmiao granite and occupy  $\leq 4$  vol% of the syenogranite phase of the batholith. Results of Rhyolite-MELTS modeling suggest that the pegmatite-forming melts can be produced through continuous fractional crystallization of the Taishanmiao granitic magma, consistent with the designation of the pegmatites as a miarolitic class, segregation-type pegmatites rather than the more common intrusive-type of pegmatite. The mineral assemblage predicted by Rhyolite-MELTS after  $\sim 96\%$  of the original granite-forming melt had crystallized consists of  $\sim 51$  vol% alkali feldspar, 34 vol% quartz, 14 vol% plagioclase, 0.1 vol% biotite, and 1 vol% magnetite, similar to the alkali feldspar + quartz dominated mineralogy of the pegmatites. Moreover, the modeled residual melt composition following crystallization of  $\sim 96\%$  of the original melt is similar to the composition of homogenized MI in quartz within the pegmatite. Rhyolite-MELTS predicts that the granite-forming melt remained volatile-undersaturated during crystallization of the batholith and contained  $\sim 6.3$  wt% H<sub>2</sub>O and  $\sim 500$  ppm CO<sub>2</sub> after  $\sim 96\%$  crystallization when the pegmatites began to develop. The Rhyolite-MELTS prediction that the melt was volatile-undersaturated at the time the pegmatites began to form, but became volatile-saturated during the early stages of pegmatite formation, is consistent with the presence of some inclusion assemblages consisting of only MI, while others contain co-existing MI and FI. The relationship between halogen (F and Cl) and Na abundances in MI is also consistent with the interpretation that the very earliest stages of pegmatite formation occurred in the presence of a volatile-undersaturated melt and that the melt became volatile saturated as crystallization progressed.

We propose a closed system, isochoric model for the formation of the pegmatites. Accordingly, the Taishanmiao granite crystallized isobarically at  $\sim 3.3$  kbar, and the pegmatites began to form at  $\sim 734$  °C and  $\sim 3.3$  kbar, after  $\sim 96\%$  of the original granitic melt had crystallized. During the final stages of crystallization of the granite, small pockets of the remaining residual melt became isolated within the enclosing granite and evolved as constant mass (closed), constant volume (isochoric) systems, similar to the manner in which volatile-rich melt inclusions in igneous phenocrysts evolve during post-entrapment crystallization under isochoric conditions. As a result of the negative volume change associated with crystallization, pressure in the pegmatite initially decreases as crystals form, and this leads to volatile exsolution from the melt phase. The changing *PTX* conditions produce a pressure-induced “liquidus deficit” that is analogous to liquidus undercooling and results in crystal growth as required to return the system to equilibrium *PTX* conditions. Owing to the complex closed system, isochoric *PVTX* evolution of the melt-crystal-volatile system, the pressure does not decrease rapidly or monotonically during pegmatite formation but, rather, gradually fluctuates such that at some stages in the evolution of the pegmatite the pressure is decreasing while at other times the pressure increases as the system cools to maintain mass and volume balance. This behavior, in turn, leads to alternating episodes of precipitation and dissolution that serve to coarsen (ripen) the crystals to produce the pegmatitic texture. The evolution of the pegmatitic melt described here is analogous to that which has been well-documented to occur in volatile-rich MI that undergo closed system, isochoric, post-entrapment crystallization.

**Keywords:** Melt inclusion, fluid inclusion, Taishanmiao batholith, liquidus deficit, volatile-saturated melt, Rhyolite-MELTS, pegmatite; Experimental Halogens in Honor of James Webster

\* E-mail: rjb@vt.edu

† OrCID 0000-0003-3801-7441

‡ Special collection papers can be found online at <http://www.minsocam.org/MSA/AmMin/special-collections.html>.

## INTRODUCTION

Granitic pegmatites are characterized by coarse- to giant-sized (centimeter to meter scale) crystals, and vary in mineralogy from simple to complex (London 2008). Considerable debate surrounds the processes that lead to the formation of pegmatite textures, and a model that explains all pegmatite characteristics has yet to be developed (Simmons and Webber 2008). Based on experimental data and observations, Jahns and Burnham (1969) suggested that exsolution of an aqueous phase from the silicate melt following extensive crystallization is the most critical step in the genesis of pegmatites, and that water saturation characterizes the transition from a granitic (phaneritic) to pegmatitic texture. However, London (2005) noted similarities in pegmatite textures and zonation produced in experiments conducted at both anhydrous and vapor-saturated conditions (London et al. 1988, 1989) and concluded that pegmatitic textures could develop in the absence of volatile-saturation. Furthermore, Fenn (1986) and London et al. (1989) asserted that a large degree of liquidus undercooling of a water-undersaturated silicate melt can produce the large crystals that are a characteristic feature of pegmatites. Despite the general consensus requiring an igneous source, it has also been suggested that pegmatitic melt could be formed by direct anatexis of rocks with appropriate composition, and this model does not require protracted fractional crystallization (Nabelek et al. 1992; Simmons et al. 1995; Falster et al. 1997).

More recently, Sirbescu et al. (2017) and Maneta and Anderson (2018) studied pegmatite formation using the hydrothermal diamond-anvil cell (HDAC). This method offers the advantage that the process can be monitored continuously and in real time to observe changes as the pegmatite texture forms. Sirbescu et al. (2017) studied pegmatite formation in the haplogranite-Li-B-H<sub>2</sub>O system in the HDAC and were able to reproduce many of the textures commonly observed in zoned pegmatites, including skeletal, graphic, unidirectional, radiating, spherulitic, massive, and replacement textures. Maneta and Anderson (2018) were able to monitor the growth of crystals in real time in their HDAC experiments and determined growth rates for quartz and alkali feldspars that ranged from 3 to 31 cm/year and 18 to 58 cm/year, respectively.

Melt (and fluid) inclusions in plutonic igneous rocks provide important information on petrologic processes (Student and Bodnar 1996; Bodnar and Student 2006; Thomas et al. 2006) and can contribute to evaluating the various models proposed for pegmatite formation (Thomas et al. 2000, 2006). In particular, the coexistence of melt inclusions (MI) and fluid inclusions (FI) (see, for example, Audétat and Petke 2003, their Fig. 3b; Thomas and Davidson 2013) provides conclusive evidence that the silicate melt was volatile-saturated at the time of inclusion trapping. Moreover, MI trapped in pegmatite minerals can be analyzed to obtain compositions of pegmatitic melt that are more reliable recorders of the melt composition during pegmatite formation compared to whole-rock compositions, owing to uncertainties in bulk compositions obtained from pegmatites with coarse and variable grain size.

The Taishanmiaio granitic batholith, located in the Eastern Qinling Orogen in Henan Province, China (Fig. 1), contains numerous small bodies with textural and mineralogical characteristics similar to those reported in granitic pegmatites and miarolitic cavities. The geology, petrology, and mineralogy of the granitic batholith have been studied in detail previously (Ye et al. 2008; Gao et al.

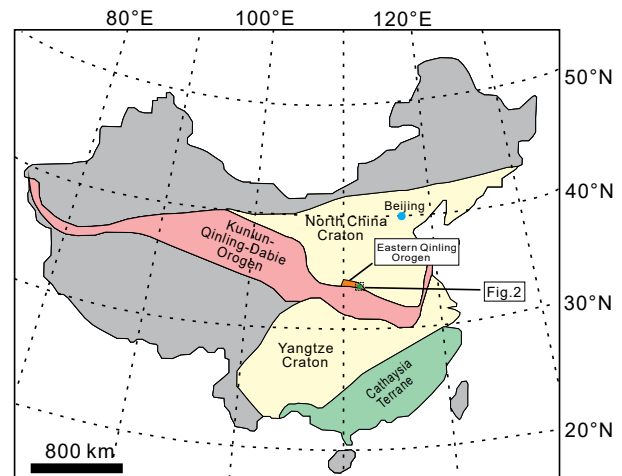


**FIGURE 1.** Simplified geologic map of China showing the location of the Taishanmiaio batholith within the Eastern Qinling Orogen (modified after Wang et al. 2016). The study area outlined by the black dashed line is shown in more detail in Figure 2. (Color online.)

2014; Qi 2014; Wang et al. 2016; Jin et al. 2018), and the results provide a solid foundation for modeling the crystallization history of the pegmatites. In this study, FI and MI in coarse quartz crystals intergrown with alkali feldspar from the Taishanmiaio pegmatites have been examined. Some inclusion assemblages (Bodnar and Student 2006) contain only melt or fluid inclusions, while other assemblages consist of co-existing MI and aqueous-carbonic FI. MI and FI were analyzed by a variety of methods, including microthermometry, Raman spectroscopy, and electron probe microanalysis that included energy-dispersive X-ray spectroscopy (EDS) and wavelength-dispersive spectroscopy (WDS), to determine the pressure-volume-temperature-composition-time (*PVTXt*) evolution of melts and aqueous fluids associated with the formation of the Taishanmiaio pegmatites. Additionally, magmatic-hydrothermal evolution in the Taishanmiaio batholith was examined by applying the Rhyolite-MELTS (Gualda et al. 2012) model, and the residual melt composition after 96% crystallization of the original melt was compared with the compositions of MI in pegmatitic quartz. The good agreement between *PVTXt* results from analysis of MI and FI and modeling predictions suggest that the Taishanmiaio pegmatites formed by the continued fractional crystallization of volatile-enriched silicate melt that evolved from the magma that produced the Taishanmiaio granite. The melt was volatile-undersaturated during the initial stages of pegmatite formation but became volatile-saturated during the early stages of pegmatite formation as a result of pressure fluctuations associated with crystallization in a closed, isochoric system. These observations have important implications concerning the role of volatile saturation and pressure fluctuations in the formation of pegmatitic textures.

Here, we use the term “pegmatite” to refer to an igneous rock composed of large (centimeter scale or larger) subhedral to euhedral crystals. Our goal is to better understand the physical and chemical conditions that cause a melt that is crystallizing an equilibrium assemblage of anhedral, medium-to-coarse grained phases (mostly quartz and alkali feldspar) in the enclosing granite to begin to form

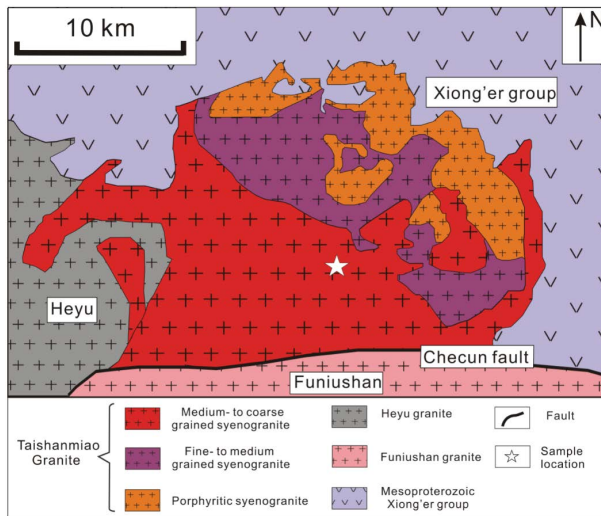


**FIGURE 2.** Simplified geologic map of the Taishanmiaio batholith in Henan Province (modified after Ye et al. 2008). Also shown by the star is the location within the batholith where the samples studied here were collected. (Color online.)

much larger subhedral crystals of those very same phases, i.e., a pegmatitic texture, with little or no apparent change in the bulk melt composition or physical environment associated with the abrupt change in crystal morphology and texture.

The Taishanmiaio pegmatites described here are thought to represent the end-stage of crystallization of the enclosing host granites and do not represent an externally derived melt that was intruded into a compositionally different and cooler host rock. As such, the pegmatite bodies studied here represent “segregations” as described by London (2008) and Candela and Blevin (1995), who describe segregation pegmatites as “lacking intrusive contacts, and are thought to represent the last volumes of residual melt in the plutons that host them (London 2008).” Moreover, the textural, mineralogical, and petrologic features place the pegmatites in the miarolitic class of pegmatites that show an abundance of open space and/or clay-filled or crystal-lined cavities. We note that London (2008) describes two different types of miarolitic pegmatites—one type is represented by segregations within shallowly emplaced granites that produce crystal-lined cavities with open space, and the other is hosted in intrusive pegmatites that are concentrically zoned or layered, such as those in the well-known San Diego County, California, pegmatite deposits. The Taishanmiaio pegmatites described here represent the former type of miarolitic pegmatite, i.e., the miarolitic class, segregation-type pegmatites described by London (2008). For simplicity, throughout this presentation, we refer to these bodies simply as “pegmatites” unless additional characterization is required for clarification.

### GEOLOGIC BACKGROUND AND SAMPLE DESCRIPTION

The Taishanmiaio batholith is located in the Eastern Qinling Orogen in Henan Province, China (Fig. 1). The orogen is part of the Qinling-Dabie orogenic belt that was formed by the collision of the North China Block and the Yangtze Craton during the Early Mesozoic (Zhang et al. 1996; Mao et al. 2002; Ratschbacher et

al. 2003). The Taishanmiaio batholith is exposed at the surface over an area of ~290 km<sup>2</sup> and intrudes to the north and east into the Proterozoic Xiong'er Group (Fig. 2), which is mainly composed of ~1.78 Ga volcanic rocks (Peng et al. 2008). At the western margin, an extension of the batholith is intruded into the slightly older Early Cretaceous Heyu granite batholith (Fig. 2) that has been dated at ~127 Ma (Mao et al. 2010). To the south, the Checun fault separates the Taishanmiaio batholith from the Mesozoic Funiushan granite batholith (Fig. 2).

The Early-Middle Cretaceous Taishanmiaio granite (125–113 Ma, Ye et al. 2008; Gao et al. 2014; Qi 2014; Wang et al. 2016) consists of three syenogranite lithologies that are differentiated based on crystal size and texture. Here, we use the term “Taishanmiaio batholith” to describe the physical intrusive body, and use the term “Taishanmiaio granite” to refer to the undifferentiated lithologies that make up the batholith and which are distinguished from each other based mostly on texture. The undifferentiated Taishanmiaio granite is classified as an aluminous, high-K, calc-alkaline A-type granite that was generated in a post-orogenic or intraplate extensional setting (Xie et al. 2007; Ye et al. 2008; Wang et al. 2013, 2016). It includes medium- to coarse-grained syenogranite, fine- to medium-grained syenogranite, and porphyritic syenogranite (Ye et al. 2008) (Fig. 2). These three phases have similar chemical compositions and mineral assemblages, although the proportions of the mineral phases differ slightly. Pegmatites and quartz veins are found in all three granite phases (Ye et al. 2008; Qi 2014). The pegmatites mostly occur as irregular or elongated features (Figs. 3a, 3c, and 3d) and occupy ~2 to 4 vol% of the syenogranite phase (Ye et al. 2008). The pegmatites are generally tens of centimeters in outcrop length and are mainly composed of coarse-grained, intergrown quartz and K-rich alkali feldspar with crystal size typically 0.5–3 cm (Figs. 3b and 3d). Open space, with faceted crystals extending into the open space, is a common feature of the pegmatites (Fig. 3c).

The samples studied here were collected from a pegmatite body that is ~70 cm long and 10–20 cm wide (Fig. 3c) and is typical of pegmatites within the Taishanmiaio medium- to coarse-grained syenogranite. In the field and in hand samples, the boundary between pegmatitic and granitic texture is easily recognized based on the abrupt change in crystal size without an associated change in mineralogy (Figs. 3a, 3c, and 3d). The melt (and fluid) inclusion assemblages studied occur in the coarse-grained quartz that is intergrown with K-feldspar (area labeled “Intergrown coarse quartz and K-feldspar” in Fig. 3c). MI are not observed in coarse quartz crystals that extend into open space and are interpreted to represent the latest stage of crystallization of the pegmatites, although FI do occur in these crystals. This suggests that either melt was not present during the final stages of quartz crystal growth or, alternatively, melt was present but was not trapped as melt inclusions. We note that the crystals are complexly intergrown and individual crystals do not show growth zoning or other macro- or microscopic features that can be used to establish a relative chronology of individual crystals, although we recognize that other methods, such as cathodoluminescence or trace element zoning, could provide such paragenetic information (Peppard et al. 2001).

MI in pegmatite quartz appears to be completely crystallized

(although we cannot exclude the possibility that some amount of glass may be present), which is typical of MI in plutonic rocks (Bodnar and Student 2006) (Figs. 4a–4c). Two-phase, liquid + vapor (L+V) FI co-exist with crystallized MI in several cases (Fig. 4c). Fluid inclusions similar to those observed co-existing with MI are also observed randomly distributed in some quartz crystals, without any associated MI (Figs. 4d and 4e). These FI are interpreted to have trapped magmatic fluid similar to the fluid trapped along with MI in other parts of the crystal. Some secondary FI along late, healed fractures were also observed (Fig. 4d), but these were not studied here. A detailed petrographic description of the MI and FI is included in the Online Material<sup>1</sup>.

#### ANALYTICAL METHODS AND MODELING

To constrain the physical conditions and geochemical processes associated with formation of the Taishanmiaog pegmatites, various methods were applied to analyze MI and FI, including microthermometry, Raman spectroscopy, and EDS and WDS analyses. In addition, the Rhyolite-MELTS algorithm (Gualda et al. 2012; Ghiorso and Gualda 2015) was applied to reconstruct the igneous evolution of the Taishanmiaog granite to test the hypothesis that the Taishanmiaog pegmatites crystallized from a late-stage (residual) melt, and thus represent segregation-type pegmatites. Details of the analytical methods are provided in Online Material<sup>1</sup>.

#### RESULTS

The H<sub>2</sub>O and CO<sub>2</sub> concentrations in the MI were estimated through a combination of analyses of the glass and vapor bubbles in MI by Raman spectroscopy. The H<sub>2</sub>O content of glass in the homogenized MI (Figs. 5a and 5b) ranges from 3.2–4.5 wt%, with an average content of 4.1 wt% and a standard deviation of ~0.5 wt% (Online Material<sup>1</sup> Table OM1; Online Material<sup>1</sup> Fig. OM3). After heating, some MI still contained crystals and/or a large vapor bubble (Fig. 5c), and these MI were assumed to have leaked or trapped multiple phases and were not selected for further analysis. Details of the analytical procedures and assumptions are included in Online Material<sup>1</sup>.

Raman analysis of the glass phase in the MI failed to detect CO<sub>2</sub>, and we have assumed that the trapped melt contains 500 ppm CO<sub>2</sub> (based on results of the Rhyolite-MELTS modeling) (see Online Material<sup>1</sup> for additional details). The assumed CO<sub>2</sub> concentration is within the range reported for MI in other silicic magmatic systems (Anderson et al. 2000; Wallace 2005). We note that the actual CO<sub>2</sub> concentration selected for the trapped melt has little effect on the conclusions reached below because we are only considering relative changes in the MI properties during pegmatite formation.

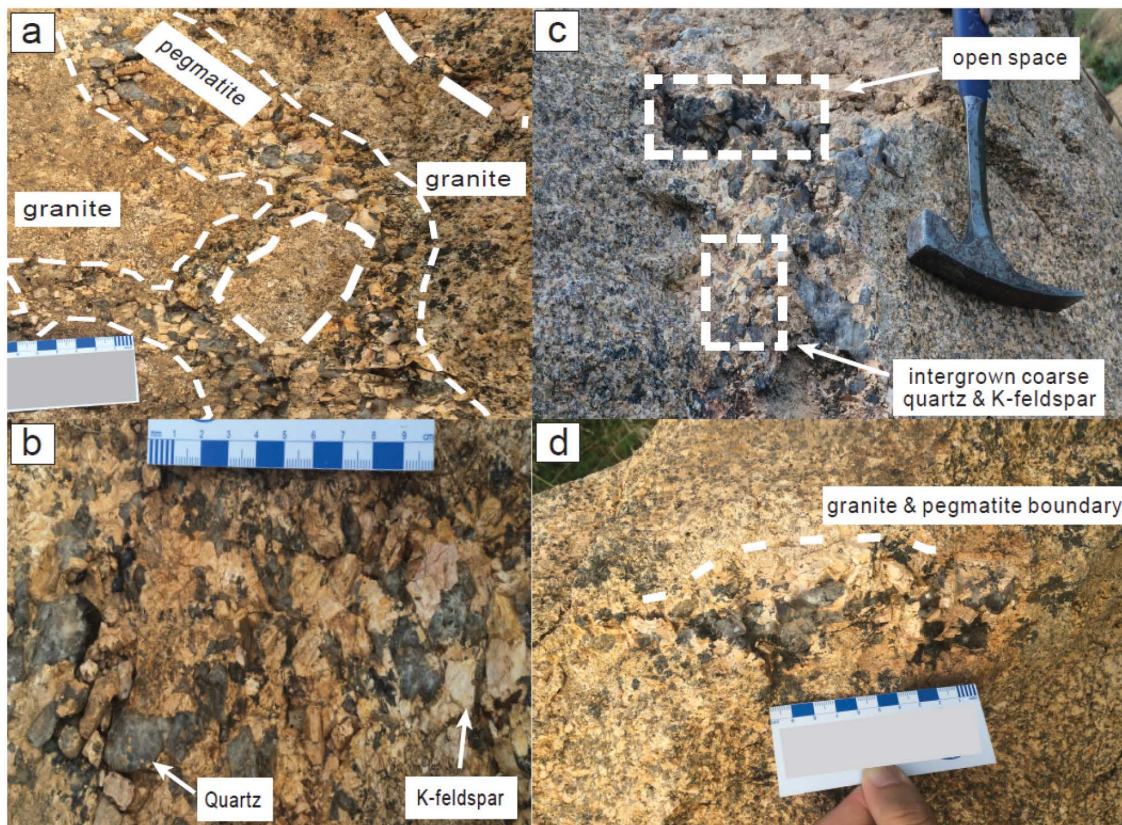
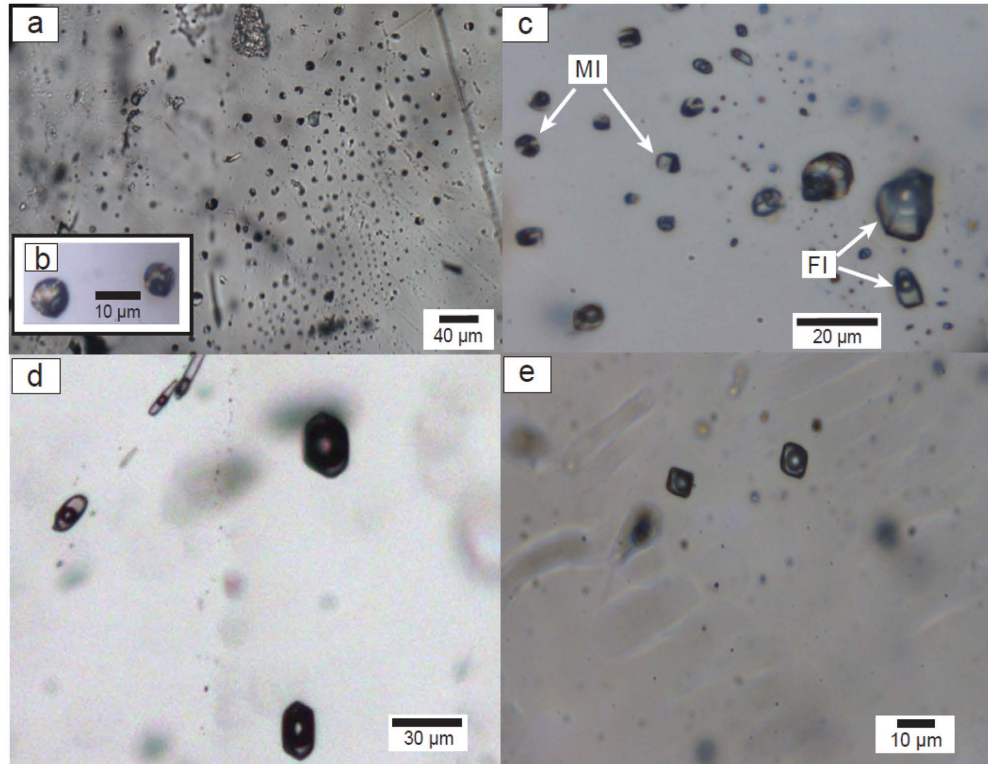


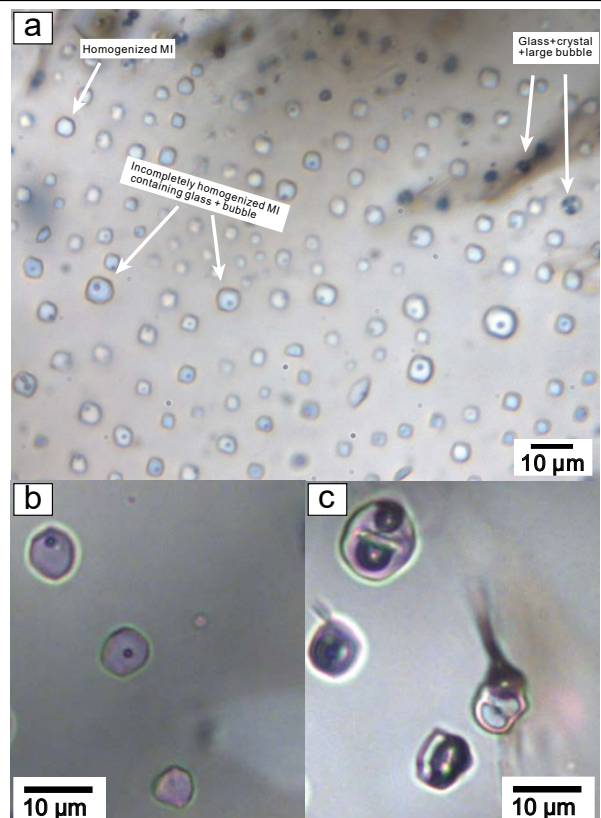
**FIGURE 3.** Photographs of pegmatite outcrops within the Taishanmiaog granite. White dashed lines in **a** and **d** denote the boundary between the coarse-grained K-feldspar and quartz assemblage in the pegmatite and the similar but finer-grained assemblage in the surrounding granite. **(a)** Pegmatite body that surrounds and envelops a granite clast. **(b)** Intergrowth of coarse-grained K-feldspar and quartz in the pegmatite, with crystal sizes ranging from ~0.5–3 cm. **(c)** The melt (and fluid) inclusion assemblages studied mostly occur in the coarse-grained quartz from the intergrowth texture shown here. Also shown is open space within the pegmatite that is interpreted to have been filled with an H<sub>2</sub>O-CO<sub>2</sub> magmatic fluid during pegmatite formation. **(d)** Pegmatite body showing the boundary between the pegmatite and surrounding granite. Note the absence of dendritic quartz that is often interpreted as evidence of undercooling that leads to formation of the pegmatitic texture in intrusive-style pegmatites. (Color online.)

► **FIGURE 4.** Photomicrographs of melt and fluid inclusions entrapped in quartz. (a) An assemblage consisting of crystallized melt inclusions outlining a crystal surface in quartz. (b) Crystallized melt inclusions containing crystals + vapor + aqueous liquid from the assemblage shown in a. (c) An inclusion assemblage consisting of coeval melt inclusions (MI) and fluid inclusions (FI) in quartz. The FI contain CO<sub>2</sub>-bearing aqueous liquid + vapor, with the vapor phase occupying ~20–50 vol% of the inclusion. (d) Secondary liquid-rich inclusions along a healed fracture and two CO<sub>2</sub>-vapor-rich, negative-crystal shaped two-phase FI in pegmatitic quartz. (e) Two negative-crystal shaped, two-phase FI that homogenized at 370 °C (left FI) and 359 °C (right FI). (Color online.)



Raman analyses of fluid inclusions that co-exist with MI in quartz crystals Z2 and A5 indicate the presence of CO<sub>2</sub> in the bubble, and only liquid H<sub>2</sub>O was detected in the liquid phase when analyzed at room temperature. The data confirm that the fluid phase in equilibrium with the melt during pegmatite formation contained both H<sub>2</sub>O and CO<sub>2</sub>. The FI homogenize to the liquid phase at 278.4 to 306.4 °C, and salinity ranges from 5.0–5.7 wt% NaCl equivalent. Homogenization temperatures of other randomly distributed FI that do not co-exist with MI (cf. Fig. 4e) range from 283 to 370 °C. As noted above, these randomly distributed FI that do not co-exist with MI do not occur along healed fractures and not of obvious secondary origin. Here, we assume that these FI were trapped at magmatic conditions when the pegmatite minerals were forming. Details concerning the microthermometric analyses are

► **FIGURE 5.** Photomicrographs of melt inclusions in crystal A5 after heating to 850 °C in the Linkam 1400XY heating stage. (a) Most of the MI are homogenized and contain glass ± a small vapor bubble occupying 0.5–2 vol% of the inclusion. MI that are completely homogenized (no vapor bubble) tend to be smaller than those that still contain a vapor bubble. Some MI contain a relatively large bubble (usually >25 vol%) as shown by the MI in the upper right. These MI likely leaked during heating or trapped some vapor along with the melt and are not considered further in the interpretation of results. (b) MI after heating to 850 °C that contain glass ± a small vapor bubble occupying 0.5–2 vol% of the inclusion. (c) MI that contain a relatively large bubble (usually >25 vol%) and crystals after heating and quenching. These and similar MI are interpreted to have leaked during heating and were not studied further. Details of the homogenization of MI are provided in Online Material<sup>1</sup>. (Color online.)



included in Online Material<sup>1</sup>.

Crystallized MI in quartz crystals A2, A5, and Z1 were analyzed by Raman spectroscopy. Owing to the fine-grained and intergrown texture of the crystals in the MI, it was generally not possible to obtain an analysis of a single phase without some contribution to the spectrum from other nearby phases, including the quartz host. Raman spectra of all MI were consistent with a mixture of quartz and mica (most likely muscovite).

EDS data were collected on 14 MI from three melt inclusion assemblages contained in 3 different quartz crystals. We emphasize that owing to the complex intergrown nature of the crystals in the pegmatite, relative ages of the three different crystals and their contained MI could not be determined. One MI from crystal A5 yielded an anomalously high-SiO<sub>2</sub> content and is interpreted to be compromised by contribution from the host quartz, or alternatively, the elevated SiO<sub>2</sub> content is the result of overheating the MI during homogenization, as described above, and is not considered further. Two MI from crystal A5 yielded high-Al<sub>2</sub>O<sub>3</sub> and -TiO<sub>2</sub> concentrations that are interpreted to reflect mixed analyses that included glass plus incompletely dissolved muscovite, as was clearly observed in 1 of the 2 MI analyzed (Online Material<sup>1</sup> Fig. OM4) and are not considered further. The remaining 11 analyses are listed in Online Material<sup>1</sup> Table OM3 along with three replicate analyses of MI from crystal Z1 collected by WDS methods.

The Rhyolite-MELTS simulations assumed a constant pressure of 3.3 kbar during crystallization, with oxygen fugacity buffered at QFM+2. From the initiation of crystallization (0%) up to ~96 wt% crystallization, the model predicts crystallization of quartz, alkali-feldspar, plagioclase, biotite, and spinel (classified as magnetite here from the simulated mineral chemical result) (Fig. 6). The predicted mineral assemblage and proportions of individual phases obtained from thermodynamic modeling are consistent with petrographic observations (Table 1). After ~96% crystallization, representing the beginning of the pegmatite stage, the melt contains 6.3 wt% H<sub>2</sub>O and 500 ppm CO<sub>2</sub> and is volatile-undersaturated. Details of the Rhyolite-MELTS simulations are included in Online Material<sup>1</sup>.

## DISCUSSION

### Is the melt that produced the Taishanmiaog pegmatites a late-stage product of felsic magma evolution?

Field and hand sample observations indicate that the Taishanmiaog pegmatites represent the miarolitic class of segregation-type pegmatites (London 2008) that crystallize from the residual melt remaining after crystallization of the bulk of the magma that produced the enclosing host granites. Candela (1997) suggests that melts are not present during the formation of miarolitic cavities in granites, and that the crystals grow directly from a magmatic

volatile phase. Conversely, several more recent studies, such as those of Audétat and Pettke (2003) and Zajacz et al. (2008), show clear evidence for the coexistence of silicate melts and aqueous fluids during formation of miarolitic cavities in granites. These differing interpretations suggest that multiple processes may be responsible for generating miarolitic cavities containing large crystals, just as various processes have been shown to produce similar pegmatitic textures.

Based on occurrences of MI and FI observed in the present study, it appears that at some times during the formation of the Taishanmiaog pegmatites only a volatile-undersaturated melt was present (perhaps early in the formation of the pegmatites), while at other times both a melt and H<sub>2</sub>O-CO<sub>2</sub> fluid phase co-existed, and at yet other times (perhaps during the latest stages of formation of the pegmatites) only an H<sub>2</sub>O-CO<sub>2</sub> fluid was present without melt. We also emphasize that it is well known among FI and MI researchers that the absence of a given type of inclusion does not necessarily indicate that the phase was not present in the system, as the mechanisms and processes of inclusion trapping are poorly understood. As such, while the presence of a given type of inclusion (MI or FI) provides solid evidence that the phase was present at the time that the inclusions were trapped, the converse is not true. As such, crystals could have grown from the fluid (non-melt) phase, even if a melt was present in the system. Thus, assemblages of FI (without MI) of indeterminate origin in some quartz crystals that extend into open space in the pegmatites could have been trapped while melt was still present, but they could also have been

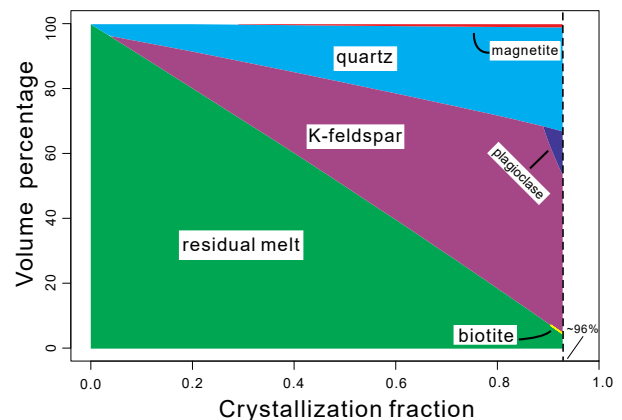


**FIGURE 6.** Mineral phases and their relative abundances (in vol%) predicted by Rhyolite-MELTS during crystallization of the granitic melt that formed the Taishanmiaog batholith. After ~96% crystallization, the predicted mineral assemblage and their relative abundances are consistent with the mineralogy of the granite in the Taishanmiaog batholith at the time that the pegmatites began to form (Table 1). (Color online.)

**TABLE 1.** Observed and predicted mineralogy of the Taishanmiaog granite

Major mineral components	Mineralogy of lithologies	Mineralogy of lithology	Mineral assemblage of [mol%] the pegmatite
	1 and 2 (vol%) <sup>a</sup>	3 (vol%) <sup>b</sup>	predicted by Rhyolite-MELTS (vol%)
K-feldspar	45–65	~50	51.1 [24.3]
Quartz	25–35	~35	33.6 [68.8]
Plagioclase	10–20	~12	14.1 [6.8]
Biotite	1–5	~2	0.1
Magnetite	minor	minor	1.0

<sup>a</sup> Lithologies 1 and 2 include the medium- to coarse-grained syenogranite and the fine- to medium-grained syenogranite. Mineral proportions are summarized from Qi (2014), Wang et al. (2016); and Jin et al. (2018).

<sup>b</sup> Lithology 3 represents the porphyritic syenogranite. Mineral proportions are summarized from Wang et al. (2016).

**TABLE 2.** Bulk rock and melt compositions for the Taishanmiao granite

Major oxide components	Range in reported bulk composition for the Taishanmiao granite <sup>b</sup> (wt%)	Starting composition used to model crystallization of Taishanmiao granite (wt%)	Residual melt composition at beginning of pegmatite formation (wt%)	Volatile-free residual melt composition at beginning of pegmatite formation (wt%)	Compositions of MI in quartz (wt%)
SiO <sub>2</sub>	70.28–78.98	75.73	69.1	73.8	78.2–81.7
TiO <sub>2</sub>	0.09–0.44	0.1	0.23	0.25	–
Al <sub>2</sub> O <sub>3</sub>	11.20–14.57	12.64	14.2	15.2	11.5–14.9
Fe <sub>2</sub> O <sub>3</sub>	–	0.60	0.24	0.26	–
FeO	1.07–2.35 <sup>a</sup>	1.09	0.27	0.29	0.5–0.8 <sup>a</sup>
MgO	0.07–0.62	0.07	0.14	0.15	–
CaO	0.21–1.23	0.42	0.95	1.0	0.1–0.5
Na <sub>2</sub> O	2.92–4.30	3.58	2.6	2.8	0.8–3.0
K <sub>2</sub> O	4.51–6	5.38	4.7	5.1	1.8–3.9
P <sub>2</sub> O <sub>5</sub>	0.01–0.11	0.02	0.49	0.52	–
F	0.02–0.5	0.03	0.74	0.79	0.3–1.4
H <sub>2</sub> O	–	0.26	6.3	–	–
CO <sub>2</sub>	–	0.0022	0.05	–	–

<sup>a</sup> Note that Total Fe is reported as FeO.

<sup>b</sup> Data summarized from Ye et al. (2008), Gao et al. (2014), Wang et al. (2016), and Jin et al. (2018).

trapped after all of the melt had crystallized.

From the initiation of crystallization (0%) to ~96% crystallization under isobaric conditions (3.3 kbar), the temperature of the magma decreases from the liquidus temperature (~1074 °C) to ~734 °C. The predicted volatile-free normalized residual melt composition after 96 wt% crystallization is 73.8 wt% SiO<sub>2</sub>, 15.2 wt% Al<sub>2</sub>O<sub>3</sub>, 5.1 wt% K<sub>2</sub>O, 2.8 wt% Na<sub>2</sub>O, 1.0 wt% CaO, 0.29 wt% FeO, 0.26 wt% Fe<sub>2</sub>O<sub>3</sub>, 0.15 wt% MgO, 0.52 wt% P<sub>2</sub>O<sub>5</sub>, and 0.79 wt% F (Table 2). The melt-free normalized mineral assemblage at this stage consists of 51.1 vol% K-feldspar, 33.6 vol% quartz, 14.1 vol% plagioclase, 0.1 vol% biotite, and 1.0 vol% magnetite (Table 1).

MI trapped in pegmatitic quartz in the Taishanmiao batholith are characterized by high silica (78.2–81.7 wt%), 13.20 wt% Al<sub>2</sub>O<sub>3</sub> (11.5–14.9 wt%), 1.90 wt% Na<sub>2</sub>O (0.8–3.0 wt%), 2.85 wt% K<sub>2</sub>O (1.8–3.9 wt%), 0.3 wt% CaO (0.1–0.5 wt%), MgO (below detection limit), and 0.65 wt% FeO (0.5–0.8 wt%). The melts are variably enriched in F (0.3–1.4 wt%) and Cl (0.03–0.30 wt%). The trapped silicate melt is peraluminous with variable but high-aluminum saturation index (A/CNK: 1.41–2.92). The model-predicted composition is similar to the peraluminous granitic composition exhibited by MI in pegmatite quartz, with some minor differences. The K<sub>2</sub>O and Al<sub>2</sub>O<sub>3</sub> contents in the modeled melt are slightly higher, and the SiO<sub>2</sub> is modestly lower than that in the analyzed MI. However, when differences in predicted and observed biotite contents are taken into consideration, the predicted lower amounts of biotite result in increased Al<sub>2</sub>O<sub>3</sub> and K<sub>2</sub>O contents and decreased SiO<sub>2</sub> content. The difference in predicted vs. observed biotite content is probably mainly responsible for the minor discrepancy in Al<sub>2</sub>O<sub>3</sub> and K<sub>2</sub>O contents between the simulated residual melt and the MI, and the elevated SiO<sub>2</sub> contents most likely reflect excess melting of quartz from the MI walls. Recognizing the minor differences described above, compositions of MI agree reasonably well with the modeled residual melt composition after ~96% crystallization at ~734 °C, and we conclude that pegmatite melt represented by the MI can be derived by extensive fractional crystallization of the Taishanmiao granitic magma.

### Pressure-temperature conditions of formation of the Taishanmiao pegmatites

The samples described here and their properties observed in the field, in hand sample and in thin section show characteristics

of the miarolitic class of segregation-type pegmatites described by London (2008). During formation of the pegmatites, some portion of the miarolitic cavity is thought to have been filled with a non-silicate (H<sub>2</sub>O-CO<sub>2</sub>) fluid phase that exsolved from the melt during the late stages of crystallization—today the volume occupied by the fluid during pegmatite formation is represented by open space within the pegmatite. While pegmatites can form over a wide range of pressures, miarolitic cavities are thought to require low-pressure formation conditions, and Candela (1997) notes that miarolitic cavities become less common with increasing formation pressure and are uncommon at crystallization pressures of 3 kbar or higher. A common textural feature of both segregation-type pegmatites and miarolitic cavities is that they both show external (heterogeneous) nucleation, whereby the crystals nucleate on an existing substrate rather than nucleating in and precipitating directly from a fluid or melt phase (homogeneous nucleation). The samples studied here consist of large quartz and K-feldspar crystals, some of which are in contact with and appear to have nucleated on the enclosing granitic substrate. The crystals are inferred to have grown into an open space, and open spaces are common in the samples as found in the field. As such, the samples described here fit into the miarolitic class of segregation-type pegmatites described by London (2008) and represent melt segregations that evolved over time to produce cavities filled with large crystals that formed in the presence of both silicate melts and an H<sub>2</sub>O-CO<sub>2</sub> fluid phase.

As noted above, the input pressure for Rhyolite-MELTS that predicts a melt composition and mineral assemblage that is most consistent with observations is ~3.3 kbar. We accept the *P-T* conditions predicted by Rhyolite-MELTS after 96% crystallization of the granitic melt (734 °C, 3.3 kbar) to represent the *P-T* conditions at the beginning of pegmatite formation, when the pegmatitic melt becomes isolated and starts to evolve as a closed, isochoric system. Moreover, we assume that the FI in pegmatitic quartz were trapped during pegmatite formation and that the melt was volatile-saturated when the FI were trapped. As such, the pressure of pegmatite formation may be constrained by the intersection of the FI isochores with the vapor-saturated solidus (Student and Bodnar 1996). Figure 7 shows the bounding isochores for fluid inclusions in quartz, calculated using the model of Steele-MacInnis (2018), and the gray-shaded area represents the complete *P-T* range of intersection of all the FI

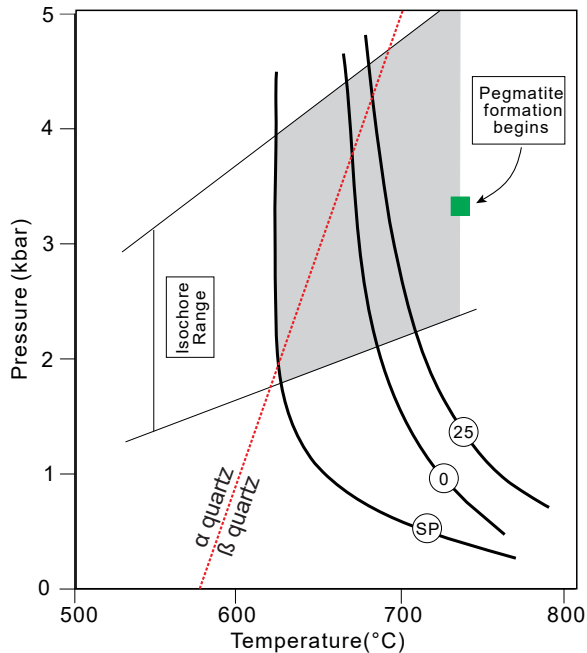


**FIGURE 7.** Estimated  $P$ - $T$  conditions for the formation of the Taishanmiaio pegmatite based on the intersection of the isochores for fluid inclusions with the Spruce Pine granitic pegmatite solidus (SP; Vaughan 1963), the  $H_2O$ -saturated granite solidus (0; Student and Bodnar 1996), and the haplogranite- $H_2O$ - $CO_2$  solidus for melt in equilibrium with a vapor phase containing 25 mol%  $CO_2$  (25; Keppler 1989). Only the isochores that intersect at the solidi at the highest and lowest pressures are shown; all other isochores intersect the solidi at pressures between these two limiting values. The green box represents the  $P$ - $T$  conditions (3.3 kbar; 734 °C) after ~96% of the melt that formed the Taishanmiaio granite had crystallized, and is interpreted to represent the  $P$ - $T$  conditions at the beginning of pegmatite formation. The gray shaded area represents the  $P$ - $T$  range defined by pressures along the FI isochores in the temperature range from 625 to 734 °C, and is interpreted to represent the range in  $P$ - $T$  conditions corresponding to pegmatite formation. Also shown are the  $\alpha/\beta$  quartz transition  $P$ - $T$  coordinates. (Color online.)

isochores (including those FI that do not co-exist with MI) with the three solidi shown. The choice of which solidus to use when interpreting the MI and FI data affects the estimated formation conditions. Based on results of Rhyolite-MELTS modeling, analysis of FI and MI in quartz, and comparison with other pegmatites, we include the  $H_2O$ -saturated granite solidus, the vapor-saturated solidus for volatile-saturated haplogranite melt in equilibrium with an  $H_2O$ - $CO_2$  fluid containing 25 mol%  $CO_2$ , and the vapor-saturated solidus for a flux-rich melt represented by the Spruce Pine Pegmatite (Fig. 7).

The fluid inclusion isochores intersect the various volatile-saturated solidi over a pressure range from ~1.7 to ~4.5 kbar (Fig. 7), and we interpret the pegmatite formation pressure to be in this broad range. The temperatures of intersection of the isochores with the volatile-saturated solidi range from about 625 to 710 °C and are broadly consistent with observations during MI microthermometry.

The results of Rhyolite-MELTS modeling and FI and MI data suggest that the Taishanmiaio pegmatites began to form at

~730 °C and ~3.3 kbar, at which point the original granitic melt had undergone ~96 wt% crystallization; pegmatite formation continued during cooling to ~625 °C. During pegmatite formation, the melt became volatile-saturated and exsolved a magmatic  $H_2O$ - $CO_2$  fluid phase.

### Evolution of the melt-volatile system during formation of the Taishanmiaio pegmatites

Various hypotheses have been put forward related to the processes and conditions required to generate a pegmatitic texture in granitic rocks. Among these, the two most commonly invoked models are that pegmatitic textures develop when a crystallizing melt reaches water saturation and exsolves a magmatic aqueous phase (Jahns and Burnham 1969), the other being that large crystals form when a water-undersaturated silicate melt undergoes a large degree of liquidus undercooling (Fenn 1986; London et al. 1989). We note that this latter interpretation applies mostly to intrusive pegmatites that form when a hotter melt is intruded into a cooler host rock.

Results of Rhyolite-MELTS modeling, combined with examination of mineral phases and bulk rock compositions and compositions of melt inclusions, suggest that the Taishanmiaio batholith transitioned from crystallization of a medium-to-coarse grained granite to abrupt formation of pegmatites having essentially the same bulk composition and mineralogy as the granite. Field and laboratory observations, combined with Rhyolite-MELTS modeling, suggest that crystallization of the batholith, including both the granite and the late pegmatites, was a continuous process with no abrupt changes in temperature or pressure. We also note that the silicate melt was volatile-saturated during at least some portion of the time when pegmatites were forming, as evidenced by  $CO_2$ -bearing aqueous FI that co-exist with MI in some assemblages (Fig. 4c).

Sodium-chloride-fluoride (Na-Cl-F) systematics observed in melt inclusions are also consistent with the interpretation that the melt became volatile-saturated during pegmatite formation. In general, halogens such as F and Cl behave as incompatible components in silicate melt systems (i.e., these elements are not incorporated into crystallizing phases) in the absence of topaz or zinnwaldite formation (Webster et al. 2004). As such, their concentrations in the melt increase as crystallization proceeds under volatile-undersaturated conditions. However, once the melt reaches volatile saturation and an aqueous phase exsolves, F and Cl show differing behavior. Experimental studies (Burnham 1967; Hards 1976; London 1987; Webster and Holloway 1987) have shown that the distribution coefficient of F,  $D_F$  (defined as the ratio of F concentration in the aqueous phase to that in the granitic melt), typically ranges from 0.1–0.4 at magmatic-hydrothermal  $P$ - $T$  conditions. This suggests that F would remain in the melt during exsolution of a magmatic aqueous phase. The silicate melt would be continuously enriched in F as fractional crystallization proceeds, even in the presence of an exsolving aqueous phase, as is observed in many natural systems (Li et al. 2017). In contrast, once volatile saturation is achieved, Cl is strongly partitioned into the aqueous phase, especially in rhyolitic systems, with  $D_{Cl}$  varying from 16 to 115 based on experiment results (Webster et al. 2009). This leads to a decrease in the Cl concentration in the silicate melt during aqueous phase exsolution.

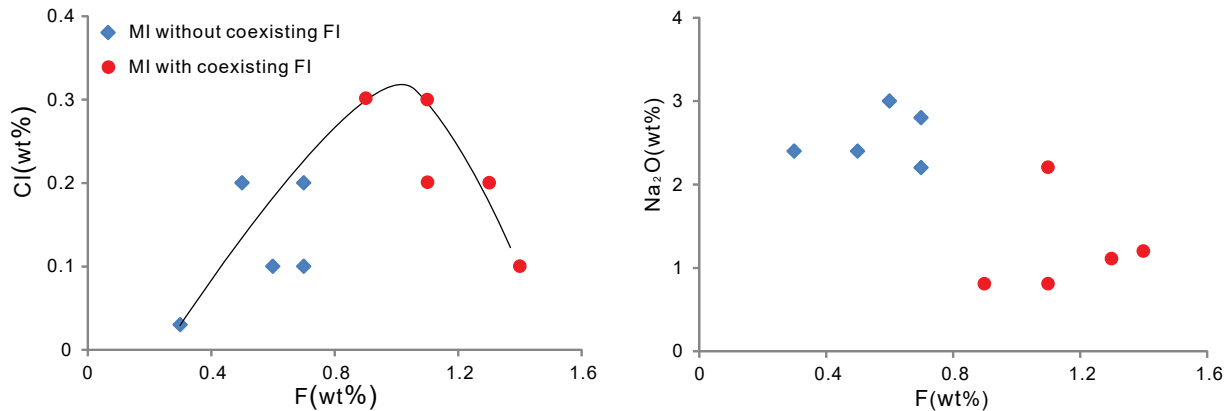


**FIGURE 8.** Relationship between the concentration of Cl (**left**) and Na (**right**) vs. F concentration in MI based on data from EDS and WDS analyses. (**left**) Cl concentration increases with increasing F concentration over the range 0.3–0.9 wt% F, after which the Cl concentration decreases with continued increase in F from 0.9 to 1.4 wt%. The change from increasing Cl with F to decreasing Cl with F is interpreted to represent the stage in the crystallization history at which the melt becomes volatile-saturated. The line is not a fitted line to the data, but rather is meant to highlight the trend of increasing Cl with F, followed by a decrease in Cl with continued increase in F concentration. (**Right**) Na content vs. F concentration measured in MI. The concentration of Na<sub>2</sub>O in MI that co-exist with FI (0.8–2.2 wt%; red dots) is lower than the Na concentration in inclusion assemblages where MI do not co-exist with FI (Na<sub>2</sub>O: 2.2–3.0 wt%; blue dots). This is consistent with the fact that Cl is likely transported from the melt into the magmatic aqueous phase as an alkali chloride (NaCl) species. (Color online.)

A correlation diagram showing the relationship between Cl and F concentrations in MI shows that the Cl concentration increases with increasing F for MI containing between about 0.3–0.9 wt% F (Fig. 8). Then, the Cl concentration decreases as F continues to increase from 0.9 to 1.4 wt%. The trend is consistent with the petrographic observation that MI with F concentrations  $\geq 0.9$  wt% are from crystal A5 that shows co-existing FI and MI, indicating that the MI trapped a volatile-saturated melt (Student and Bodnar 1999). Previously, Webster et al. (2015) showed that Cl concentrations in the fluid-absent melt increase as the magma fractionally crystallizes and reaches its maximum or solubility limit when the melt becomes saturated in hydrosaline liquid and/or vapor. Likewise, the Cl concentration in the MI of this study shows a positive correlation with F in the range 0.3–0.9 wt% F as melt crystallization proceeds and reaches a maximum of 0.3 wt% Cl when an aqueous phase starts to exsolve from the melt. Then, as magma continues to evolve, F increases from 0.9 to 1.4 wt% in the MI that is coeval with the aqueous fluid inclusions, while Cl decreases from 0.3 to 0.1 wt%. The sodium concentration in the MI is also lower in MI that trapped a volatile-saturated melt (Fig. 8), consistent with transport of Na in the fluid as an NaCl complex. Thus, Cl and Na vs. F trends observed here are consistent with the interpretation that the melt was volatile-undersaturated during the early stages of pegmatite formation but became volatile-saturated at some point during the formation of the pegmatites.

#### Model for formation of the Taishanmiaog pegmatites

As noted above, the two most commonly invoked models for the formation of pegmatites involve liquidus undercooling (Fenn 1986; London et al. 1989) or volatile saturation (Jahns and Burnham 1969) of the melt. These models generally apply to intrusive pegmatites that form when a hotter melt is intruded into a cooler host rock, and the melt cools quickly to temperatures well

below its equilibrium liquidus (or solidus) temperature. Internal nucleation of phases occurs and the crystals grow rapidly in this non-equilibrium environment to produce a pegmatitic texture.

In petrology, the term “liquidus undercooling” is used to describe the process whereby a magma (melt-crystal±volatile system) existing at equilibrium  $P$ - $T$  conditions on the liquidus for that system is abruptly inserted into a lower temperature environment such that the system is no longer at equilibrium. This, in turn, can lead to rapid crystal growth driven by a change in melt composition as the system attempts to return to an equilibrium state at the new liquidus  $P$ - $T$  conditions. Alternatively, if the shift to lower temperatures is sufficiently large that the new temperature is in the subsolidus region, all of the melt may crystallize as a result of undercooling.

While decreasing the temperature (liquidus undercooling) represents one mechanism to drive the magma system away from equilibrium, it is not the only process that can cause a system that is initially at equilibrium to suddenly experience a non-equilibrium environment (Grove and Till 2015). For example, pressure-induced crystallization may result if the pressure decreases for a system with a liquidus or solidus curve that shows a negative slope in  $P$ - $T$  space, such as the volatile-saturated solidus in most volatile-bearing silicate melt systems, including the granite- $\text{H}_2\text{O}\pm\text{CO}_2$  system (see Burnham and Davis 1971; Keppler 1989). Similarly, crystallization may result if the composition of one or more of the phases in the system changes. As an example, consider a haplogranite melt that is in equilibrium with an  $\text{H}_2\text{O}$ - $\text{CO}_2$  fluid phase containing 25 mol%  $\text{CO}_2$ . If the  $\text{CO}_2/\text{H}_2\text{O}$  ratio of the fluid that co-exists with the melt were to suddenly increase while the temperature and pressure remain constant as, for example, during flux of mantle-sourced  $\text{CO}_2$ -rich fluid into a magma undergoing crystallization, the temperature of the system would be lower than the temperature on the liquidus corresponding to the new  $\text{CO}_2$ -enriched fluid composition at the same pressure. This would

drive crystallization to bring the melt back into equilibrium with the new fluid composition (see Keppler 1989, his Fig. 2). These various processes that can lead to non-equilibrium conditions to produce a “liquidus deficit,” as defined by Labrosse (2014). Accordingly, a “liquidus deficit” is the result of any change in the physical or chemical properties of a system that causes the system to depart from equilibrium liquidus conditions, and the units of the liquidus deficit are Kelvins (or degrees Celsius), identical to the units for liquidus undercooling. Thus, a change in composition or pressure that leads to a liquidus deficit would be described in terms of the difference in temperature on the equilibrium liquidus before the perturbation, and the temperature of the system after the temperature, pressure, or composition of the system has changed to move the system away from equilibrium.

The model proposed here for the formation of the Taishanmiao pegmatites involves the development of a pressure-induced, vapor-saturated liquidus deficit that promotes episodic crystal dissolution and precipitation in an attempt to return the system to equilibrium conditions. This interpretation is consistent with results presented by Candela (1997), who reports that “the formation of miarolitic cavities requires bubble growth during magma ascent and decompression.” We propose that “decompression” (decreasing pressure), as well as increasing pressure, can occur in the absence of magma ascent if the miarolitic cavity represents a closed, isochoric system.

The Taishanmiao pegmatites represent miarolitic class, segregation-type pegmatites that form in the very latest stages of crystallization of a larger granitic body. During the waning stages of crystallization of the granite, pockets of melt became isolated and enclosed within a rigid container represented by the previously crystallized granite surrounding the melt pocket. As crystallization of the pegmatites proceeds in this closed (constant mass), isochoric (constant volume) system, the *PVTX* conditions within the pegmatite body evolve in a manner that diverges from that of the larger granitic body. The model proposed here for the *PVTX* evolution of the melt remaining after ~96% of the granite-forming melt has crystallized is analogous to the *PVTX* evolution of a melt inclusion trapped in an igneous phenocryst. We apply those same principles here to infer the *PVTX* evolution of the pegmatite melt. We assume that the melt from which the pegmatite forms is represented by the melt that is present after ~96% of the original granitic melt has crystallized, in agreement with both field observations and results of Rhyolite-MELTS modeling. We further assume that the total volume of the system melt + crystals + vapor remains constant during pegmatite formation. Thus, the melt pocket (pegmatite) represents a closed (constant mass), isochoric (constant volume) system.

The composition of the residual melt remaining after ~96% crystallization of the original granitic melt is listed in Table 2, and this is the starting composition for formation of the pegmatites. Results of the Rhyolite-MELTS model suggest that the pegmatites began to form at about ~734 °C, and microthermometric results suggest that pegmatite formation continued to ~625 °C. The mineral assemblage predicted to form during crystallization of the residual melt consists of 24.3 mol% K-spar, 68.8 mol% quartz, 6.8 mol% plagioclase plus minor biotite and magnetite (Table 1). As crystals begin to form in the very earliest stages of pegmatite formation, the volume occupied by crystals +

remaining melt is less than that occupied by the melt before crystallization began because the crystals are more dense (occupy a smaller volume) than the melt from which they precipitated. We assume that the proportions of minerals that are forming are the same as the mineral proportions in the pegmatites (Table 1), and the volume change during crystallization may be calculated from the volume of fusion of the minerals, multiplied by their molar proportions. The volumes of fusion used to calculate the volume change are: microcline (9.75 cm<sup>3</sup>/mol);  $\beta$ -quartz (3.85 cm<sup>3</sup>/mol); albite (8.64 cm<sup>3</sup>/mol) (Lange and Carmichael 1990). We note that most of the inferred *P-T* range of formation of the pegmatites is in the  $\beta$ -quartz field, rather than the  $\alpha$ -quartz field (Fig. 7). Accordingly, the mineral-averaged volume of fusion for the pegmatite melt is 5.6 cm<sup>3</sup>/mol of melt crystallized. That is, the volume occupied by crystals + melt decreases by 5.6 cm<sup>3</sup> for every mole of melt that crystallizes. We assume that the volume of the pegmatite is equal to the volume of melt before crystals began to form, i.e., the system is isochoric; as such, the decrease in the volume of the system as melt crystallizes (melt → crystals) requires the formation of a void space in the cavity that is analogous to the shrinkage bubble that forms in a melt inclusion during post-entrapment crystallization on the inclusion walls. The formation of the shrinkage bubble requires that the pressure in the MI decrease and this results in a liquidus deficit—i.e., the new pressure is not the pressure corresponding to the liquidus at the temperature of the pegmatite body. This, in turn, leads to crystal growth combined with exsolution of volatiles from the melt into the shrinkage volume, resulting in an increase in pressure in the cavity (Fig. 9). The decrease in pressure and concomitant decrease in volatile solubility in the melt, and decrease in the amount of melt available to dissolve the volatiles as a result of crystallization, are processes that are well known in the magmatic-hydrothermal community and are referred to as “first boiling” and “second boiling,” respectively. Exsolution of volatiles from the melt ceases once the pressure in the pegmatite has stabilized at the pressure required to maintain equilibrium.

The conceptual model for the formation of the Taishanmiao pegmatites assumes a starting melt composition predicted by Rhyolite-MELTS after ~96% crystallization of the original granitic melt (Table 2). As such, Rhyolite-MELTS predicts that the residual melt has a broadly rhyolitic (granitic) composition and contains 6.3 wt% H<sub>2</sub>O and 500 ppm CO<sub>2</sub>. At 3.3 kbars and 734 °C, the melt is volatile undersaturated and the VolatileCalc solubility simulator (Newman and Lowenstern 2002) predicts that a rhyolite composition melt would become volatile-saturated and contain 6.3 wt% H<sub>2</sub>O and 500 ppm CO<sub>2</sub> when the pressure decreases to 2.653 kbar. Additionally, the H<sub>2</sub>O-CO<sub>2</sub> vapor phase in equilibrium with the melt at these conditions (734 °C, 2.653 kbar) would contain 20.4 mol% CO<sub>2</sub> and 79.6 mol% H<sub>2</sub>O. The density of the vapor phase calculated using the equation of state for H<sub>2</sub>O-CO<sub>2</sub> of Connolly and Bodnar (1983) would be 0.618 g/cm<sup>3</sup>.

Developing a rigorous quantitative model to calculate the exact *P-T* evolution of the pegmatite is beyond the scope of this study. However, we have conducted some simple mass and volume balance calculations to constrain the *P-T* evolution of the pegmatite during its formation, applying the same

methodology that has been used successfully to model post-entrapment crystallization of volatile-bearing melt inclusions (Steele-MacInnis et al. 2011) and H<sub>2</sub>O-saturated haplogranite melts (Student and Bodnar 1996). Steele-MacInnis et al. (2011) developed a quantitative model that predicts the *P-T* evolution of a melt inclusion based on *PVTX* and thermodynamic data for the system albite-H<sub>2</sub>O. As crystallization proceeds, the volume of the shrinkage bubble (vapor bubble) is equal to the difference in the volume of albite melt and crystals at the *P-T* conditions of interest. Accordingly, the volume of fusion of albite is 8.64 cm<sup>3</sup>/mol (Lange and Carmichael 1990). That is, for each mole of albite that crystallizes in the melt inclusion, a void space of 8.64 cm<sup>3</sup> is generated. Stated differently, assuming a melt molar volume of 112.83 cm<sup>3</sup>/mol and an albite molar volume of 104.13 cm<sup>3</sup>/mol (Lange and Carmichael 1990), the volume occupied by the crystal is ~7.7 vol% smaller than that of the melt from which it crystallized. The pressure in the MI at any *P-T* condition is a function of the volume of the void space generated by crystallization, the amount and composition

of the volatile phase that exsolves from the melt as a result of the pressure decrease and melt crystallization and the relative difference between the molar volume of the volatile phase and the partial molar volumes of H<sub>2</sub>O and CO<sub>2</sub> in the melt. As such, the partial molar volumes of H<sub>2</sub>O and CO<sub>2</sub> in a granitic melt are estimated to be ~18 cm<sup>3</sup>/mol for H<sub>2</sub>O (Burnham and Davis 1971) and ~34 cm<sup>3</sup>/mol for CO<sub>2</sub> (Lange and Carmichael 1990). For comparison, the molar volume of H<sub>2</sub>O at 700 °C ranges from 36.1 cm<sup>3</sup>/mol at 2 kbar to 26.0 cm<sup>3</sup>/mol at 4 kbar. Similarly, the molar volume of CO<sub>2</sub> ranges from 69.2 to 50.1 cm<sup>3</sup>/mol over this same pressure range. Assuming ideal mixing in the exsolved vapor phase, the volume occupied by H<sub>2</sub>O in the vapor phase (assuming a pure H<sub>2</sub>O composition) ranges from ~45 to 100% greater than the volume when dissolved in the melt. Similarly, the volume occupied by the CO<sub>2</sub> vapor phase is ~47 to 103 vol% larger than the volume in the melt phase. These differences in partial molar volumes compared to molar volumes, combined with the pressure dependence of the partitioning behavior of H<sub>2</sub>O and CO<sub>2</sub> between the melt and co-existing vapor, lead to

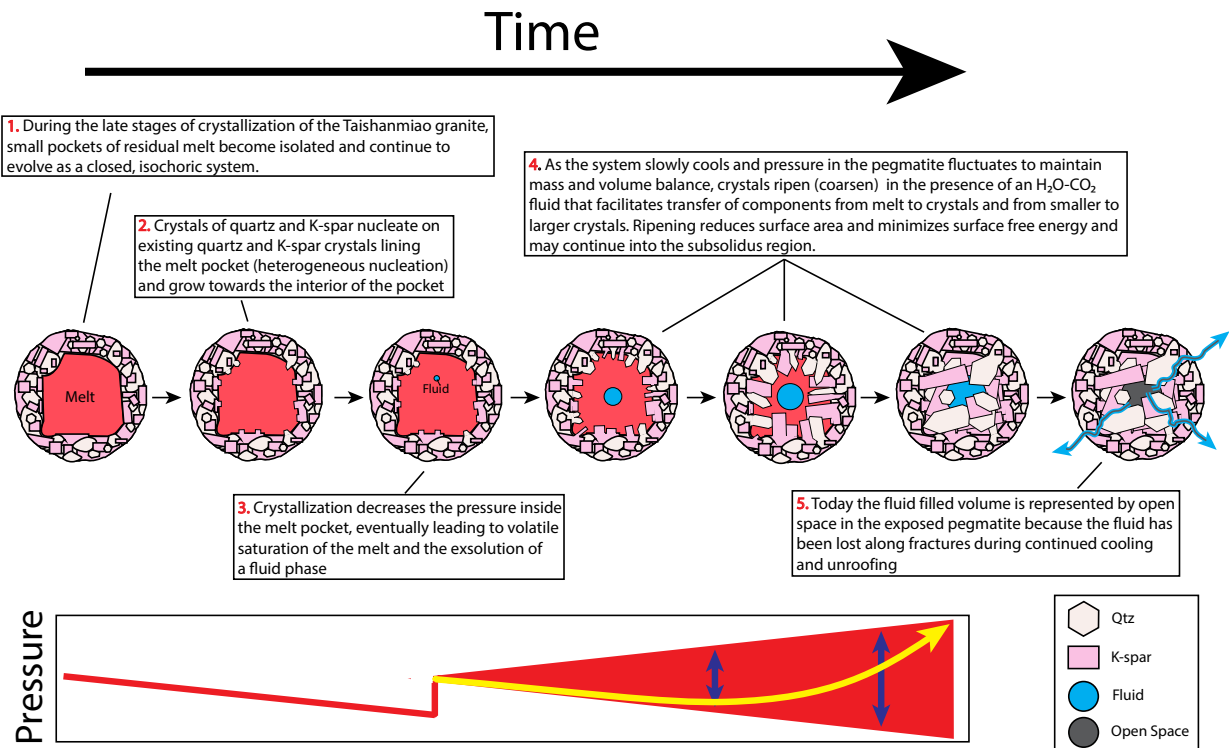


**FIGURE 9.** Schematic representation of the conceptual model proposed for formation of the Taishanmiao pegmatites. At 734 °C and 3.3 kbar, residual melt that remains after crystallization of ~96% of the Taishanmiao granite becomes isolated and continues to evolve as a closed, isochoric system (Stage 1). The melt at this stage contains 6.3 wt% H<sub>2</sub>O and 500 ppm CO<sub>2</sub> and is volatile-undersaturated. During the initial phase cooling, crystals nucleate on preexisting crystals on the walls (heterogeneous nucleation; Stage 2) and this, in turn, generates a shrinkage bubble (Stage 3) because the volume occupied by the crystals is ~7.7 vol% smaller than the volume of melt from which the crystals grew owing to the volume of fusion. The formation of the shrinkage bubble and the decrease in pressure causes a liquidus deficit and moves the *PVTX* conditions within the pegmatite-forming melt away from the equilibrium liquidus. This, in turn promotes crystal growth and an H<sub>2</sub>O-CO<sub>2</sub> fluid continues to exsolve from the melt in an attempt to return to an equilibrium state. Owing to the complex relationship between pressure, volatile solubility in the melt, and the H<sub>2</sub>O-CO<sub>2</sub> ratio in the fluid in a closed, isochoric system, the pressure in the MI fluctuates until a new equilibrium pressure is achieved, resulting in episodes of dissolution and growth of the crystals in the pegmatite (Stage 4). Ripening (coarsening) leads to development of fewer, larger crystals to reduce the surface area and surface free energy, and this results in the pegmatitic texture that characterizes miarolitic class, segregation-type pegmatites. At some later subsolidus stage (Stage 5), fractures intersect the fluid-filled cavity and the H<sub>2</sub>O-CO<sub>2</sub> escapes, leaving behind a cavity containing large crystals and a void space. (Color online.)

complex trends in the  $P$ - $T$  evolution within the MI. As such, Steele-MacInnis et al. (2011) report that the internal pressure in a melt inclusion that trapped a  $\text{CO}_2$ -saturated albite melt at 1500 bars and 1165 °C decreases from the pressure at trapping (1500 bars) to <500 bars as the amount of melt crystallized increases from 0 to 25 wt%. In the case of this simple system, as melt begins to crystallize, a shrinkage bubble forms in the MI owing to the smaller volume of crystals relative to the volume of melt before crystallization. This, in turn, leads to a pressure decrease and loss of volatiles from the melt that drives the  $PTX$  conditions further from the equilibrium conditions, promoting additional crystallization to drive the conditions back toward the  $\text{CO}_2$ -saturated solidus, which in turn promotes additional fluid loss from the melt to the vapor phase and a concomitant decrease in pressure. These two competing effects, decreasing pressure and volatile loss from the melt into the vapor that drive the conditions away from the equilibrium conditions and crystallization that works to drive conditions back toward equilibrium, continue until a steady-state condition is reached whereby the proportions and compositions of melt, crystals, and vapor are in equilibrium at some new set of  $PTX$  condition. Conversely, during post-entrapment crystallization of an albite melt containing only  $\text{H}_2\text{O}$ , the pressure in the MI increases along the  $\text{H}_2\text{O}$ -saturated solidus until crystallization is complete. This same behavior was reported by Student and Bodnar (1996) for crystallization in the haplogranite- $\text{H}_2\text{O}$  system. Finally, Steele-MacInnis et al. (2011) report that during closed system isochoric crystallization of an albite melt containing both  $\text{H}_2\text{O}$  and  $\text{CO}_2$ , the pressure in the MI initially decreases as mostly  $\text{CO}_2$  is exsolved, followed by an increase in pressure as the exsolving fluid becomes more  $\text{H}_2\text{O}$ -rich. We propose that this same process that leads to a complex  $P$ - $T$  evolution within MI undergoing crystallization in a closed, isochoric system is applicable to the formation of the miarolitic class, segregation-type pegmatites in the Taishanmiao granite.

At any temperature in the range from ~725 to ~625 °C, representing the assumed range of pegmatite formation in this study, the physical and chemical conditions that satisfy mass and volume balance based on known solubilities of  $\text{H}_2\text{O}$  and  $\text{CO}_2$  in silicate melts, the partitioning behavior of  $\text{H}_2\text{O}$  and  $\text{CO}_2$  between melt and vapor as a function of temperature and pressure, and the density of the exsolved vapor, may be calculated. As such, at 734 °C, mass and volume balance can be achieved over the pressure range 2320 to 4836 bars, and as crystallization proceeds, the pressure in the pegmatite must increase to maintain mass and volume balance (Online Material<sup>1</sup> Table OM4). As temperature decreases, the pressure range over which mass and volume balance may be achieved decreases, such that at 675 °C mass and volume balance are only possible at pressures of 2225 to 2255 (Online Material<sup>1</sup> Table OM4). At temperatures lower than 675 °C the pressure range over which mass and volume balance are possible again increases, and at 625 °C balance constraints can be satisfied between 1737 and 2155 bars. Importantly during cooling from 734 to 675 °C, pressure in the cavity must increase as crystallization proceeds to maintain mass and volume balance, whereas at temperatures <675 °C pressure in the cavity must decrease as crystallization proceeds to maintain mass and volume balance (Online Material<sup>1</sup> Table OM4). It is this pressure cycling in the cavity that occurs as the temperature slowly

decreases that leads to the liquidus deficit and the concomitant episodic dissolution and precipitation of minerals that results in ripening (coarsening) to produce the pegmatitic texture, as described below.

The pressure-driven liquidus deficit model described here may explain some inconsistencies related to an undercooling-driven model for pegmatite formation in some cases. In discussing textures of granites in magmatic-hydrothermal ore-forming systems, Candela (1997) notes that while undercooling may be valid in more shallow systems, “magmas at deeper levels, or magmas in regions of high flow, will cool more slowly and acquire an equilibrium [i.e., finer-grained?] texture.” Candela (1997) also notes that rounded cores of quartz “eyes” (phenocrysts) in these deposits suggest that at some stage in its growth history, the quartz experienced an episode of dissolution, followed by continued growth. Similar resorption of quartz phenocrysts in the Red Mountain, Arizona, porphyry copper deposit was observed by Bodnar and Student (2006; their Figs. 1–15). Candela (1997) relates the resorption and rounding of quartz eyes to changes in the water content of the melt, but we emphasize here that pressure-induced liquidus deficits could produce this same result. Candela (1997) also notes that owing to the inverse relationship between nucleation rate and crystal growth rate, undercooling can produce both a pegmatitic (coarse-grained) and aplitic (fine-grained) texture. Thus, during the initial pressure decrease in the pegmatite volume that results when crystallization begins, a fine-grained mixture of quartz and K-feldspar may be precipitated, and with time, as the  $P$ - $T$  conditions in the pegmatite volume fluctuate, the crystals may undergo ripening (coarsening) to produce the pegmatite texture (Fig. 9). Moreover, evidence for the early formation of finer-grained crystals that coarsen as a result of fluctuating dissolution and precipitation processes may not be preserved in the final texture, as suggested by Sirbescu et al. (2017), who report that “early products of crystallization may be hidden or reprocessed by superimposed crystal generations, recrystallization, and deformation.”

Based on petrographic studies of the Taishanmiao granite, combined with thermodynamic simulation of the crystallization history of the Taishanmiao granite-forming melt, and petrographic and compositional analyses of MI and FI in pegmatite quartz, the  $PVTXt$  conditions associated with the formation of the Taishanmiao pegmatite can be summarized. After ~96% of the original Taishanmiao felsic melt had crystallized at ~3.3 kbar to produce an igneous rock with a phaneritic texture, small pockets of residual melt became isolated and evolved as a closed (constant mass), isochoric (constant volume) system, and the  $P$ - $T$  path within the melt pockets diverged from that of the enclosing host granite (Fig. 9). While the pegmatite melts remained in thermal equilibrium with the surrounding host granite, the pressure in the melt pockets varied in a complex manner in response to crystallization because the volume occupied by the crystals was less than that of the melt from which they precipitated. The pressure fluctuations resulted in a liquidus deficit (analogous to undercooling) whereby the melt and crystals in the pegmatite were no longer in equilibrium with the new  $P$ - $T$  environment. This drove crystallization to change the melt and  $\text{H}_2\text{O}$ - $\text{CO}_2$  fluid composition in an attempt to return

the system to an equilibrium condition. As the temperature of the pegmatite decreased over time, the response to varying pressure in the pockets led to episodes of mineral growth and dissolution, which served to coarsen the grain size to reduce total surface area and minimize surface free energy. The model proposed here that large crystals may be generated by ripening (coarsening) of an originally fine-grained mixture is analogous to that which is commonly observed during microthermometric analysis of fluid inclusions (Online Material Fig. OM6).

The transition from the formation of a coarse-grained granite to the formation of pegmatites is temporally associated with the evolution from a volatile-undersaturated to a volatile-saturated melt. However, while the generation of an H<sub>2</sub>O-CO<sub>2</sub> volatile phase within the pegmatite may have facilitated the movement of mineral-forming components from the melt to the site of crystallization, we do not suggest that the generation of a volatile phase was necessary for pegmatite formation. Even in a dry (anhydrous and CO<sub>2</sub>-free) melt, the pressure in the system will decrease during constant mass, constant volume evolution owing to the volume of fusion that results in a decrease in total volume of melt + crystals.

While the presence of an H<sub>2</sub>O-CO<sub>2</sub> volatile phase is not required to cause the pressure to fluctuate in a closed, isochoric system undergoing crystallization, the volatile phase does facilitate and promote crystal growth. As reported by Maneta and Anderson (2018), who experimentally studied the crystallization of H<sub>2</sub>O-saturated granitic melts, "The experimental results underscore the important role of water as a medium for the transport of essential elements such as Si, Al, Na, and K from the silicate melt to the newly formed crystals." Moreover, Zajac et al. (2008) analyzed co-existing melt and fluid inclusions in quartz crystals from miarolitic cavities in several granitic to intermediate composition plutons and found significant concentrations of Al, Na, and K in the fluid inclusions. For example, the following ranges in average concentrations of these elements from 13 different melt/fluid inclusion assemblages were reported: Al = 635 to 27 796 ppm; Na = 12 147 to 109 418 ppm; K = 6885 to 124 871 ppm. These results emphasize the significant carrying-capacity of the magmatic-hydrothermal fluids present during the formation of the crystals in the miarolitic cavities and suggest that a volatile phase plays a critical role in transferring elements from the melt to the growing crystal surfaces.

The presence of volatiles also affects the viscosity of the melt phase that, in turn, affects the movement of crystal-forming components by either diffusion or advection, or both, in the evolving melt-volatile system. Audétat and Keppler (2004) showed that adding ~5 wt% H<sub>2</sub>O to an albite melt at 800 °C decreased the viscosity by about eight orders of magnitude, and with 10 wt% H<sub>2</sub>O the viscosity is more similar to that of pure H<sub>2</sub>O at the same conditions than it is to that of the anhydrous melt. Similarly, Bartels et al. (2011) report that granitic melts containing a few weight percent of Li<sub>2</sub>O, F, B<sub>2</sub>O<sub>3</sub>, and P<sub>2</sub>O<sub>5</sub> had viscosities at 773 K that were similar to those of water-saturated granitic melts at 973–1023 K. While we do not believe that melt viscosity had a significant effect on the formation of the Taishanmiao pegmatites, the lowered viscosities would favor the transfer and re-distribution of dissolved species within the melt-crystal-fluid system.

## IMPLICATIONS

The petrogenesis of pegmatites has intrigued professional mineralogists, petrologists, and geochemists for at least the past century, and serious mineral collectors continuously seek the elusive mineralized cavity filled with giant crystals. Two different processes to explain the formation of large crystals in granitic rocks are supported to a greater or lesser extent by experimental studies. In one case, pegmatites are interpreted to form when a crystallizing melt achieves water saturation, while the other popular model suggests undercooling as the mechanism associated with pegmatite formation. Both of these processes likely contribute to the formation of the more common intrusive-type pegmatites that are generated when a hotter melt is intruded into a cooler host rock.

Here, we document that MI and FI contained within pegmatite minerals provide a record of the crystallization history during pegmatite formation. Coexisting MI and FI confirm that the melts became volatile-saturated during pegmatite formation and provide information on the composition of melts and fluids that exsolved from the melts—these data are not otherwise obtainable.

The pegmatites studied here represent the miarolitic class of segregation-style pegmatites that are the result of in situ crystallization of the last remnants of residual melt remaining after the larger enclosing and cogenetic igneous body has almost completely crystallized. Field and compositional data support the interpretation that the Taishanmiao pegmatites began to form after ~96% crystallization of the host granite and the melt became saturated in volatiles shortly after the pegmatites began to form. Given the environment and mode of formation of these bodies, the undercooling model for pegmatite formation is not supported as it is difficult to envision a scenario that could generate significant temperature differences between the pegmatite melt and the surrounding, cogenetic granitic body. However, the petrological consequences of undercooling can be achieved by other means, including variations in the pressure and/or the composition of the system. Thus, a liquidus deficit may be related to changes in the temperature, or pressure, or composition of the magmatic system, and here we provide a model for the generation of a pressure-induced liquidus deficit that drives crystallization in a closed system. It is unclear if the pegmatitic (very coarse-grained) texture observed today was generated during the initial precipitation of quartz and K-feldspar in the pegmatite volume or if a fine-grained mixture of these phases was originally precipitated and subsequently underwent coarsening (ripening) to reduce total crystal surface area to minimize surface free energy (Fig. 9). We suggest the conclusions and the model described here may be applicable to other miarolitic class, segregation style pegmatitic bodies elsewhere.

## ACKNOWLEDGMENTS

The authors dedicate this contribution to the memory of James (Jim) D. Webster. Jim provided valuable advice to Y.Y. concerning melt inclusions, and Y.Y. was originally scheduled to work with Jim in his laboratory. When Jim became aware of his illness, he contacted R.J.B. and asked if he could accept Yabin as a visiting Ph.D. student. This gesture epitomizes Jim's unselfish nature and desire to help others, even when he was facing serious health issues. R.J.B. and Jim were friends and professional colleagues for almost four decades, and during the last several years, co-taught (along with Leonid Danyushevsky, Maria Luce Frezzotti, and Benedetto De Vivo) a highly successful short course on Fluids in the Earth. R.J.B. very much misses the many discussions of science, politics, and world affairs that Jim and he shared over food and beer at many locations around the world.

While it is a common courtesy to acknowledge and thank reviewers for their comments and suggestions related to a manuscript, we believe that special recogni-

tion should go to the reviewers of this paper, including Rainer Thomas and Mona Sirbescu. Their insightful yet kind criticisms of the earlier version of this paper led us to step back and take a more careful and critical look at our samples and to specifically consider more carefully the type of pegmatite we were dealing with. Much of our earlier interpretation was based on what we now recognize was an incorrect assumption that the Taishanmiaog pegmatites were similar to the more commonly studied intrusive pegmatites. Questions from the reviewers about the relationships between our pegmatites and conventional miarolitic cavities in granitic rocks and the nature of the pegmatite-host rock contact led us to re-think and develop what we now believe is a more scientifically robust interpretation of the pegmatites. We offer our very sincere thanks to the reviewers for opening our eyes!

### FUNDING AND TECHNICAL ASSISTANCE

Sampling and petrographic section preparation was supported by the National Nonprofit Institute Research Grant of the Chinese Academy of Geological Sciences (YYWF201711). We thank Charles Farley for providing technical assistance with Raman analyses. Eszter Sendula helped with the FI and MI microthermometric analyses. Luca Fedele provided assistance with sample preparation for EMP analyses of MI and I-Ming Chou provided several helpful suggestions to Y.Y.

Y.Y. acknowledges the support of Chinese Scholarship Council. This material is based in part on work supported by the National Science Foundation under grant number EAR-1624589 to R.J.B. Any use of trade, firm, or product names is for descriptive purposes only and does not imply endorsement by the U.S. Government.

### REFERENCES CITED

- Anderson, A.T., Davis, A.M., and Lu, F. (2000) Evolution of Bishop Tuff rhyolitic magma based on melt and magnetite inclusions and zoned phenocrysts. *Journal of Petrology*, 41, 4449–4473.
- Armstrong, J.T. (1988) Quantitative analysis of silicate and oxide minerals: Comparison of Monte Carlo, ZAF and Phi-Rho-Z procedures. In D.E. Newbury, Ed., *Microbeam Analysis*, p. 239–246. San Francisco Press, California.
- Audétat, A., and Keppeler, H. (2004) Viscosity of fluids in subduction zones. *Science*, 303, 513–516.
- Audétat, A., and Pettke, T. (2003) The magmatic-hydrothermal evolution of two barren granites: A melt and fluid inclusion study of the Rito del Medio and Canada Pinabete plutons in northern New Mexico (U.S.A.). *Geochimica et Cosmochimica Acta*, 67, 97–121.
- Bartels, A., Vetere, F., Holtz, F., Behrens, H., and Linnen, R.L. (2011) Viscosity of flux-rich pegmatitic melts. *Contributions to Mineralogy and Petrology*, 162, 51–60.
- Berkési, M., Hidas, K., Guzmics, T., Dubessy, J., Bodnar, R.J., Szabó, C., Vajna, B., and Tsunogae, T. (2009) Detection of small amounts of H<sub>2</sub>O in CO<sub>2</sub>-rich fluid inclusions using Raman spectroscopy. *Journal of Raman Spectroscopy*, 40, 1461–1463.
- Bodnar, R.J., and Frezzotti, M.L. (2020) Microscale chemistry: Raman analysis of fluid and melt inclusions. *Elements*, 16, 201–205.
- Bodnar, R.J., and Student, J.J. (2006) Melt inclusions in plutonic rocks: Petrography and microthermometry. In J.D. Webster, Ed., *Melt Inclusions in Plutonic Rocks*, 1–25. Mineralogical Association of Canada, Montreal, Québec.
- Burnham, C.W. (1967) Hydrothermal fluids at the magmatic stage. *Geochemistry of Hydrothermal Ore Deposits*, 34–76.
- Burnham, C.W., and Davis, N.F. (1971) The role of H<sub>2</sub>O in silicate melts; I, PVT relations in the system NaAlSi<sub>3</sub>O<sub>8</sub>-H<sub>2</sub>O to 10 kilobars and 1000 °C. *American Journal of Science*, 270, 54–79.
- Candela, P.A. (1997) A review of shallow, ore-related granites: textures, volatiles, and ore metals. *Journal of Petrology*, 38, 1619–1633.
- Candela, P.A., and Blevin, P.L. (1995) Do some miarolitic granites preserve evidence of magmatic volatile phase permeability? *Economic Geology*, 90, 2310–2316.
- Connolly, J.A.D., and Bodnar, R.J. (1983) A modified Redlich-Kwong equation of state for H<sub>2</sub>O-CO<sub>2</sub> mixtures: Application to fluid inclusion studies. *EOS*, 64, 350.
- Creaser, R.A., and White, A.J. (1991) Yardea Decite—large-volume, high-temperature felsic volcanism from the Middle Proterozoic of South Australia. *Geology*, 19, 48–51.
- Donovan, J., Kremser, D., Fournelle, J., and Goemann, K. (2015) Probe for EPMA: Acquisition, automation and analysis, version 11: Eugene, Oregon, Probe Software, Inc., <http://www.probesoftware.com>
- Drouin, D., Couture, A.R., Joly, D., Tastet, X., Aimez, V., and Gauvin, R. (2007) CASINO V2.42—a fast and easy-to-use modeling tool for scanning electron microscopy and microanalysis users. *Scanning: The Journal of Scanning Microscopies*, 29, 92–101.
- Esposito, R., Klebesz, R., Bartoli, O., Klyukin, Y., Moncada, D., Doherty, A., and Bodnar, R.J. (2012) Application of the Linkam TS1400XY heating stage to melt inclusion studies. *Open Geosciences*, 4, 208–218.
- Falster, A., Simmons, W.B., and Webber, K. (1997) The origin of evolved LCT-type granitic pegmatites in the Hoskin Lake granite-pegmatite field, Florence Co. Wisconsin. IAVCEI General Assembly.
- Fenn, P.M. (1986) On the origin of graphic granite. *American Mineralogist*, 71, 325–330.
- Gao, X.Y., Zhao, T.P., Bao, Z.W., and Yang, A.Y. (2014) Petrogenesis of the early Cretaceous intermediate and felsic intrusions at the southern margin of the North China Craton: Implications for crust-mantle interaction. *Lithos*, 206–207, 65–78.
- Ghiorso, M.S., and Gualda, G.A.R. (2015) An H<sub>2</sub>O-CO<sub>2</sub> mixed fluid saturation model compatible with rhyolite-MELTS. *Contributions to Mineralogy and Petrology*, 169, 1–30.
- Goldstein, R.H., and Reynolds, T.J. (1994) Systematics of fluid inclusions in diagenetic minerals. SEPM Society for Sedimentary Geology, 31, 199.
- Grove, T.L., and Till, C.B. (2015) Melting the Earth's upper mantle. In H. Sigurdsson, Ed., *The Encyclopedia of Volcanoes*, 35–47. Academic Press.
- Gualda, G.A.R., Ghiorso, M.S., Lemons, R.V., and Carley, T.L. (2012) Rhyolite-MELTS: A modified calibration of MELTS optimized for silica-rich, fluid-bearing magmatic systems. *Journal of Petrology*, 53, 875–890.
- Hards, N. (1976) Distribution of elements between the fluid phase and silicate melt phase of granites and nepheline syenites. *Progress in Experimental Petrology*, 3, 88–90.
- Helgeson, H.C. (1969) Thermodynamics of hydrothermal systems at elevated temperatures and pressures. *American Journal of Science*, 267, 729–804.
- Henke, B.L., Lee, P., Tanaka, T.J., Shimabukuro, R.L., and Fujikawa, B.K. (1982) Low-energy X-ray interaction coefficients: Photoabsorption, scattering, and reflection: E= 100–2000 eV Z= 1–94. *Atomic Data and Nuclear Data Tables*, 27, 1–144.
- Huebner, J., and Woodruff, M.E. (1985) Chemical compositions and critical evaluation of microprobe standards available in the Reston microprobe facility, 2331–1258. U.S. Geological Survey.
- Jahns, R.H., and Burnham, C.W. (1969) Experimental studies of pegmatite genesis; I. A model for the derivation and crystallization of granitic pegmatites. *Economic Geology*, 64, 843–864.
- Jin, C., Gao, X.Y., Chen, W.T., and Zhao, T.P. (2018) Magmatic-hydrothermal evolution of the Donggou porphyry Mo deposit at the southern margin of the North China Craton: Evidence from chemistry of biotite. *Ore Geology Reviews*, 92, 84–96.
- Keppeler, H. (1989) The influence of the fluid phase composition on the solidus temperatures in the haplogranite system NaAlSi<sub>3</sub>O<sub>8</sub>-KAlSi<sub>3</sub>O<sub>8</sub>-SiO<sub>2</sub>-H<sub>2</sub>O-CO<sub>2</sub>. *Contributions to Mineralogy and Petrology*, 102, 321–327.
- Kucharczyk, S., Sitarz, M., Zajac, M., and Deja, J. (2018) The effect of CaO/SiO<sub>2</sub> molar ratio of CaO-Al<sub>2</sub>O<sub>3</sub>-SiO<sub>2</sub> glasses on their structure and reactivity in alkali activated system. *Spectrochimica Acta Part A: Molecular and Biomolecular Spectroscopy*, 194, 163–171.
- Labrosse, S. (2014) Thermal and compositional stratification of the inner core. *Comptes Rendus Geoscience*, 346, 119–129.
- Lamadrid, H., Lamb, W., Santosh, M., and Bodnar, R.J. (2014) Raman spectroscopic characterization of H<sub>2</sub>O in CO<sub>2</sub>-rich fluid inclusions in granulite facies metamorphic rocks. *Gondwana Research*, 26, 301–310.
- Lange, R.L., and Carmichael, I.S. (1990) Thermodynamic properties of silicate liquids with emphasis on density, thermal expansion and compressibility. *Reviews in Mineralogy and Geochemistry*, 24, 25–64.
- Li, S., Li, J., Chou, I.M., Jiang, L., and Ding, X. (2017) The formation of the Yichun Ta-Nb deposit, South China, through fractional crystallization of magma indicated by fluid and silicate melt inclusions. *Journal of Asian Earth Sciences*, 137, 180–193.
- London, D. (1987) Internal differentiation of rare-element pegmatites: Effects of boron, phosphorus, and fluorine. *Geochimica et Cosmochimica Acta*, 51, 403–420.
- (2005) Granitic pegmatites: an assessment of current concepts and directions for the future. *Lithos*, 80, 281–303.
- (2008) *Pegmatites*. 347 p. The Canadian Mineralogist Special Publication, Québec, Canada.
- London, D., Hervig, R.L., and Morgan, G.B. (1988) Melt-vapor solubilities and elemental partitioning in peraluminous granite-pegmatite systems: experimental results with Macusani glass at 200 MPa. *Contributions to Mineralogy and Petrology*, 99, 360–373.
- London, D., Morgan, G.B., and Hervig, R.L. (1989) Vapor-undersaturated experiments with Macusani glass+H<sub>2</sub>O at 200 MPa, and the internal differentiation of granitic pegmatites. *Contributions to Mineralogy and Petrology*, 102, 1–17.
- Maneta, V., and Anderson, A.J. (2018) Monitoring the crystallization behavior of water-saturated granitic melts in real time using the hydrothermal diamond anvil cell. *Contributions to Mineralogy and Petrology*, 173, 83. <https://doi.org/10.1007/s00410-018-1509-7>.
- Mao, J.W., Goldfarb, R.J., Zhang, Z., Xu, W., Qiu, Y., and Deng, J. (2002) Gold deposits in the Xiaojinling-Xiong'er shan region, Qinling Mountains, central China. *Mineralium Deposita*, 37, 306–325.
- Mao, J.W., Xie, G.Q., Pirajno, F., Ye, H.S., Wang, Y.B., Li, Y.F., Xiang, J.F., and Zhao, H.J. (2010) Late Jurassic–Early Cretaceous granitoid magmatism in Eastern Qinling, central-eastern China: SHRIMP zircon U-Pb ages and tectonic implications. *Australian Journal of Earth Sciences*, 57, 51–78.
- McMillan, P., Piriou, B., and Navrotsky, A. (1982) A Raman spectroscopic study of glasses along the joints silica-calcium aluminate, silica-sodium aluminate, and silica-potassium aluminate. *Geochimica et Cosmochimica Acta*, 46, 2021–2037.
- Miller, C.F., McDowell, S.M., and Mapes, R.W. (2003) Hot and cold granites? Implications of zircon saturation temperatures and preservation of inheritance. *Geology*, 31, 529–532.
- Moore, L.R., Gazel, E., Tuohy, R., Lloyd, A.S., Esposito, R., Steele-MacInnis, M., Hauri, E.H., Wallace, P.J., Plank, T., and Bodnar, R.J. (2015) Bubbles matter: An assessment of the contribution of vapor bubbles to melt inclusion volatile budgets. *American Mineralogist*, 100, 806–823.
- Morgan, G.B., and London, D. (1996) Optimizing the electron microprobe analysis of hydrous alkali aluminosilicate glasses. *American Mineralogist*, 81, 1176–1185.
- (2005) Effect of current density on the electron microprobe analysis of alkali

- aluminosilicate glasses. *American Mineralogist*, 90, 1131–1138.
- Morizet, Y., Brooker, R.A., Iacono-Marziano, G., and Kjarsgaard, B.A. (2013) Quantification of dissolved CO<sub>2</sub> in silicate glasses using micro-Raman spectroscopy. *American Mineralogist*, 98, 1788–1802.
- Nabelek, P.L., Russ-Nabelek, C., and Denison, J. (1992) The generation and crystallization conditions of the Proterozoic Harney Peak leucogranite, Black Hills, South Dakota, USA: Petrologic and geochemical constraints. *Contributions to Mineralogy and Petrology*, 110, 173–191.
- Newman, S., and Lowenstern, J.B. (2002) VolatileCalc: A silicate melt-H<sub>2</sub>O-CO<sub>2</sub> solution model written in Visual Basic for Excel. *Computers and Geosciences*, 28, 597–604.
- Peng, P., Zhai, M., Ernst, R.E., Guo, J., Liu, F., and Hu, B. (2008) A 1.78 Ga large igneous province in the North China craton: The Xiong'er Volcanic Province and the North China dyke swarm. *Lithos*, 101, 260–280.
- Peppard, B.T., Steele, I.M., Davis, A.M., Wallace, P.J., and Anderson, A.T. (2001) Zoned quartz phenocrysts from the rhyolitic Bishop Tuff. *American Mineralogist*, 86, 1034–1052.
- Qi, Y. (2014) Petrogenesis of Laojunshan and Taishanmiaio Granite Plutons in Eastern Qinling, central China. 50 p. M.Sc. thesis, University of Science and Technology of China, Hefei (in Chinese with English abstract).
- Ratschbacher, L., Hacker, B.R., Calvert, A., Webb, L.E., Grimmer, J.C., McWilliams, M.O., Ireland, T., Dong, S., and Hu, J. (2003) Tectonics of the Qinling (Central China): Tectonostratigraphy, geochronology, and deformation history. *Tectonophysics*, 366, 1–53.
- Roedder, E. (1984) Fluid Inclusions, vol. 12. Reviews in Mineralogy, Mineralogical Society of America, Chantilly, Virginia.
- Severs, M.J., Azbej, T., Thomas, J.B., Mandeville, C.W., and Bodnar, R.J. (2007) Experimental determination of H<sub>2</sub>O loss from melt inclusions during laboratory heating: Evidence from Raman spectroscopy. *Chemical Geology*, 237, 358–371.
- Simmons, W.B., and Webber, K.L. (2008) Pegmatite genesis: state of the art. *European Journal of Mineralogy*, 20, 421–438.
- Simmons, W.B., Foord, E., Falster, A., and King, V. (1995) Evidence for an anatectic origin of granitic pegmatites, western Maine, U.S.A. Geological Society of America Annual Meeting, New Orleans, Abstract Program, 27, A411.
- Sirbescu, M.-L.C., Schmidt, C., Veksler, I.V., Whittington, A.G., and Wilke, M. (2017) Experimental crystallization of undercooled felsic liquids: Generation of pegmatitic texture. *Journal of Petrology*, 58, 539–568.
- Steele-MacInnis, M. (2018) Fluid inclusions in the system H<sub>2</sub>O-NaCl-CO<sub>2</sub>: An algorithm to determine composition, density and isochore. *Chemical Geology*, 498, 31–44.
- Steele-MacInnis, M., Esposito, R., and Bodnar, R.J. (2011) Thermodynamic model for the effect of post-entrapment crystallization on the H<sub>2</sub>O-CO<sub>2</sub> systematics of vapor-saturated, silicate melt inclusions. *Journal of Petrology*, 52, 2461–2482.
- Stern, S.M., and Bodnar, R.J. (1984) Synthetic fluid inclusions in natural quartz I. Compositional types synthesized and applications to experimental geochemistry. *Geochimica et Cosmochimica Acta*, 48, 2659–2668.
- Student, J.J., and Bodnar, R.J. (1996) Melt inclusion microthermometry: Petrologic constraints from the H<sub>2</sub>O-saturated haplogranite system. *Petrology*, 4, 291–306.
- (1999) Synthetic fluid inclusions XIV: Co-existing silicate melt and aqueous fluid inclusions in the haplogranite-H<sub>2</sub>O-NaCl-KCl system. *Journal of Petrology*, 40, 1509–1525.
- Thomas, R. (2000) Determination of water contents of granite melt inclusions by confocal laser Raman microprobe spectroscopy. *American Mineralogist*, 85, 868–872.
- Thomas, R., and Davidson, P. (2013) The missing link between granites and granitic pegmatites. *Journal of Geosciences*, 58, 183–200.
- Thomas, R., Webster, J.D., and Heinrich, W. (2000) Melt inclusions in pegmatite quartz: Complete miscibility between silicate melts and hydrous fluids at low pressure. *Contributions to Mineralogy and Petrology*, 139, 394–401.
- Thomas, R., Webster, J.D., and Davidson, P. (2006) Understanding pegmatite formation: The melt and fluid inclusion approach. *Melt Inclusions in Plutonic Rocks*, 36, 189–210.
- Vaughan, D. (1963) The crystallization ranges of the Spruce Pine and Harding pegmatites, 61 p. M.Sc. thesis, The Pennsylvania State University.
- Wallace, P.J. (2005) Volatiles in subduction zone magmas: Concentrations and fluxes based on melt inclusion and volcanic gas data. *Journal of Volcanology and Geothermal Research*, 140, 217–240.
- Wang, X.X., Wang, T., and Zhang, C.L. (2013) Neoproterozoic, Paleozoic, and Mesozoic granulite magmatism in the Qinling Orogen, China: Constraints on orogenic process. *Journal of Asian Earth Sciences*, 72, 129–151.
- Wang, C., Chen, L., Bagas, L., Lu, Y., He, X., and Lai, X. (2016) Characterization and origin of the Taishanmiaio aluminous A-type granites: implications for Early Cretaceous lithospheric thinning at the southern margin of the North China Craton. *International Journal of Earth Sciences*, 105, 1563–1589.
- Watson, E.B., and Harrison, T.M. (1983) Zircon saturation revisited: temperature and composition effects in a variety of crustal magma types. *Earth and Planetary Science Letters*, 64, 295–304.
- Webster, J.D., and Holloway, J.R. (1987) Partitioning of halogens between topaz rhyolite melt and aqueous and aqueous-carbonic fluids. *Geological Society of America, Abstracts with Program*, 19, 884.
- Webster, J.D., Thomas, R., Förster, H.J., Seltmann, R., and Tappen, C. (2004) Geochemical evolution of halogen-enriched granite magmas and mineralizing fluids of the Zinnwald tin-tungsten mining district, Erzgebirge, Germany. *Mineralium Deposita*, 39, 452–472.
- Webster, J.D., Tappen, C.M., and Mandeville, C.W. (2009) Partitioning behavior of chlorine and fluorine in the system apatite–melt–fluid. II: Felsic silicate systems at 200 MPa. *Geochimica et Cosmochimica Acta*, 73, 559–581.
- Webster, J.D., Vetere, F., Botcharnikov, R.E., Goldoff, B., McBirney, A., and Doherty, A.L. (2015) Experimental and modeled chlorine solubilities in aluminosilicate melts at 1 to 7000 bars and 700 to 1250 °C: Applications to magmas of Augustine Volcano, Alaska. *American Mineralogist*, 100(2-3), 522–535.
- Xie, G., Mao, J., Li, R., Ye, H., Zhang, Y., Wan, Y., Li, H., Gao, J., and Zheng, R. (2007) SHRIMP zircon U-Pb dating for volcanic rocks of the Daying Formation from Baofeng basin in eastern Qinling, China and its implications. *Acta Petrologica Sinica*, 23, 2387–2396 (in Chinese with English abstract).
- Ye, H., Mao, J., Xu, L., Gao, J., Xie, G., Li, X., and He, C. (2008) SHRIMP zircon U-Pb dating and geochemistry of the Taishanmiaio aluminous A-type granite in western Henan Province. *Geological Review*, 54, 699–711 (in Chinese with English abstract).
- Zajacz, Z., Halter, W.E., Pettke, T., and Guillong, M. (2008) Determination of fluid/melt partition coefficients by LA-ICP-MS analysis of co-existing fluid and silicate melt inclusions: Controls on element partitioning. *Geochimica et Cosmochimica Acta*, 72, 2169–2197.
- Zhang, G., Meng, Q., Yu, Z., Sun, Y., Zhou, D., and Guo, A. (1996) The orogenic process and dynamic analysis of the Qinling Orogen. *Science in China Series D*, 39, 1–9 (in Chinese).

MANUSCRIPT RECEIVED MAY 23, 2020

MANUSCRIPT ACCEPTED DECEMBER 10, 2020

MANUSCRIPT HANDLED BY JUSTIN FILIBERTO

### Endnote:

<sup>1</sup>Deposit item AM-21-107637, Online Materials. Deposit items are free to all readers and found on the MSA website, via the specific issue's Table of Contents (go to [http://www.minsocam.org/MSA/AmMin/TOC/2021/Oct2021\\_data/Oct2021\\_data.html](http://www.minsocam.org/MSA/AmMin/TOC/2021/Oct2021_data/Oct2021_data.html)).